

Atmospheric Constraints on the Surface UV Environment of Mars at 3.9 Ga Relevant to Prebiotic Chemistry

Sukrit Ranjan^{1,2}, Robin Wordsworth^{3,4}, Dimitar D. Sasselov¹

February 1, 2022

ABSTRACT

Recent findings suggest Mars may have been a clement environment for the emergence of life, and may even have compared favorably to Earth in this regard. These findings have revived interest in the hypothesis that prebiotically important molecules or even nascent life may have formed on Mars and been transferred to Earth. UV light plays a key role in prebiotic chemistry. Characterizing the early Martian surface UV environment is key to understanding how Mars compares to Earth as a venue for prebiotic chemistry.

Here, we present two-stream multi-layer calculations of the UV surface radiance on Mars at 3.9 Ga, to constrain the surface UV environment as a function of atmospheric state. We explore a wide range of atmospheric pressures, temperatures and compositions, corresponding to the diversity of Martian atmospheric states consistent with available constraints. We include the effects of clouds and dust. We calculate dose rates to quantify the effect of different atmospheric states on UV-sensitive prebiotic chemistry.

We find that for normative clear-sky CO₂-H₂O atmospheres, the UV environment on young Mars is comparable to young Earth. This similarity is robust to moderate cloud cover: thick clouds ($\tau_{cloud} \geq 100$) are required to significantly affect the Martian UV environment, because cloud absorption is degenerate with atmospheric CO₂. On the other hand, absorption from SO₂, H₂S, and dust is nondegenerate with CO₂, meaning if these constituents build up to significant levels, surface UV fluence can be suppressed. These absorbers have spectrally variable absorption, meaning that their presence affects prebiotic pathways in

¹Harvard-Smithsonian Center for Astrophysics, Cambridge, MA 02138, USA

²60 Garden Street, Mail Stop 10, Cambridge, MA 02138, USA; sranjan@cfa.harvard.edu; 617-495-5676

³Harvard Paulson School of Engineering and Applied Sciences, Harvard University, Cambridge, MA 02140, USA

⁴Department of Earth and Planetary Sciences, Harvard University, Cambridge, MA 02140, USA

different ways. In particular, high SO_2 environments may admit UV fluence that favors pathways conducive to abiogenesis over pathways unfavorable to it. However, better measurements of the spectral quantum yields of these pathways are required to evaluate this hypothesis definitively.

Subject headings: Radiative Transfer, Origin of Life, Mars, UV Radiation, Prebiotic Chemistry

1. Introduction

Recent findings suggest that young Mars may have been a clement environment for the emergence of life. Analysis of Curiosity imaging of sedimentary rock strata deposited 3.2-3.6 Ga (Grotzinger et al. 2015) suggest individual lakes were stable on ancient Mars for 100-10,000 years, with fluvial features laid down over 10,000-10 million years assuming formation rates corresponding to modern Earth. Similarly, Curiosity measurements of olivine and magnetite at Yellowknife crater are consistent with aqueous conditions at near-neutral pH for thousands to hundreds of thousands of years in the Noachian, with an oxidant supply that could be an energy source (Bristow et al. 2015). In general, the geologic evidence is compelling that liquid water, a requirement for life as we know it, was present on Mars at least transiently in the Noachian (Wordsworth 2016).

The young Mars may also have been a favorable environment for prebiotic chemistry (chemistry relevant to the origin of life). Meteorite analysis has detected boron in Martian clays, important for abiogenesis since borate minerals can stabilize ribose and catalyze other prebiotic chemistry reactions (see Stephenson et al. 2013 and sources therein). Mars may also have enjoyed greater availability of prebiotically important phosphate than Earth (Adcock et al. 2013). Climate models suggest liquid water was transient on Mars (Wordsworth et al. 2013), which suggests the evidence of wet/dry cycles. Such cycles are useful for prebiotic chemistry: aqueous eras are beneficial for the formation of biotic monomers, while dry eras tend to concentrate feedstock molecules and aid monomer polymerization (Benner et al. 2015), relevant to the formation of nucleotides and amino acids (Patel et al. 2015). Finally, the putative dryness of Mars and the potential acidity of its early aqueous environment owing to dissolved carbonic acid from a CO_2 -dominated atmosphere, suggest molybdate, which is suggested to catalyze formation of prebiotically important sugars such as ribose, may have been stable on Mars (Benner et al. 2015, 2010). Hence, there is growing interest in the possibility that prebiotically important molecules may have been produced on Mars (Benner 2013), and even the hypothesis that life may have originated on Mars and been seeded to Earth (Kirschvink and Weiss 2002; Gollihar et al. 2014; Benner et al. 2015).

Ultraviolet (UV) light plays a key role in prebiotic chemistry. UV photons can dissociate molecular bonds, produce ionic species, and excite molecules. These properties mean that UV light can stress prebiotic molecules (Sagan 1973), but also that UV light can power synthetic prebiotic photochemistry. UV light has been invoked in prebiotic chemistry as diverse as the origin of chirality (Rosenberg et al. 2008), the synthesis of amino acid precursors (Sarker et al. 2013), and the polymerization of RNA (Mulkiđjanian et al. 2003).

The last decade has seen breakthroughs in long-standing problems in prebiotic chemistry such as the discovery of plausible mechanisms for the abiotic formation of activated pyrimidine ribonucleotides (Powner et al. 2009), the synthesis of short (2- and 3-carbon) sugars (Ritson and Sutherland 2012), and a reaction network generating precursors for a range of prebiotically important molecules including lipids, amino acids, and ribonucleotides (Patel et al. 2015). These pathways all require UV light to function. In experiments, line sources such as low-pressure mercury lamps with monochromatic 254 nm emission are often used to simulate the incident UV radiation. However, prebiotic UV radiance in CO₂-dominated terrestrial-type atmospheres should instead be characterized by access to broadband fluence (Ranjan and Sasselov 2017). The difference can have a significant impact on prebiotic chemistry (Ranjan and Sasselov 2016), and there is a growing awareness in the prebiotic community of the importance of characterizing the wavelength dependence of proposed prebiotic pathways and/or using broadband sources in simulations (Rapf and Vaida 2016). Consequently, it is important to constrain the UV environment on the surface of Mars at epochs relevant to potential prebiotic chemistry on a spectral (wavelength-dependent) basis.

In this work, we use a two-stream multilayer radiative transfer model to constrain the surface UV environment on young Mars (3.9 Ga). We calculate the surface radiance as a function of solar zenith angle (SZA), surface albedo (A), and atmospheric composition. Our model can calculate absorption and scattering due to 8 gaseous species (CO₂, H₂O, CH₄, SO₂, H₂S, O₂, and O₃) and 3 particulate species (H₂O ice, CO₂ ice, and Martian dust). Earlier analyses have focused on clear-sky "case studies" for the atmospheric composition; we instead explore the full range of Martian atmospheric states consistent with available geological data and climate/photochemical modelling for the Martian atmosphere. We convolve the calculated surface radiance spectra against action spectra corresponding to two different simple photochemical reactions (one useful to prebiotic chemistry, and one detrimental) that may have been important during the era of abiogenesis, and integrate the result to compute the biologically effective dose rate (BED) and estimate the impact of these parameters on prebiotic chemistry.

In Section 2, we discuss previous work on this topic. In Section 3, we describe our radiative transfer model and its inputs and assumptions. Section 4 presents the surface

radiances calculated from our model as a function of Martian atmospheric state, and Section 5 discusses the implications for prebiotic chemistry. Section 6 summarizes our findings.

2. Background

Recognizing the importance of UV light to life (though mostly in the context of a stressor), previous workers have placed constraints on the primitive Martian surface UV environment. In this section, we present a review of previous work on this topic, and discuss how our work differs from them.

Cockell (2000) calculate the Martian surface flux at 3.5 Ga assuming solar input of $0.75 \times$ modern, and an atmosphere composed of 1 bar CO_2 and 0.1 bar N_2 . They compute their radiative transfer in a cloud-free atmosphere using a monolayer two-stream approximation with Delta-Eddington closure. They ignore water absorption, but a dust optical depth of 0.1 is assumed, as is a Lambertian surface with surface albedo $A = 0.1$. Cockell (2000) report the total irradiance as a function of solar time (equator at equinox) as well as the biologically-weighted¹ irradiance for DNA inactivation and photosystem damage, but not the spectral irradiance (for the early Mars case). They find the DNA inactivation-weighted irradiance to be comparable for their models of Early Mars and Early Earth, leading them to suggest that from a UV perspective the two worlds were comparably habitable.

Rontó et al. (2003) calculate the Martian surface flux at 3.5 Ga from 200-400 nm. They assume a 1-bar CO_2 atmosphere overlying volatilizable surface H_2O , and ran it through the PHOEBE photochemical model to generate atmospheric profiles for the other molecules that would be generated. They found a significant population of spectrally absorbing O_2 , O_3 , and NO_2 would be generated, including an ozone shield comparable to the modern Earth. They evaluated radiative transfer for both a pure CO_2 atmosphere, as well as for an atmosphere with the trace species calculated in their photochemical model. Their UV radiative transfer models assumes pure absorption and ignores scattering. In this formulation, Rontó et al. (2003) calculated Rayleigh scattering cross-sections but treated them as absorption cross-sections. This approach strongly overestimates attenuation at scattering wavelengths. It is consequently unsurprising that Rontó et al. (2003) report strong attenuation of surface UV fluence for both model atmosphere cases. in the full photochemical model case, fluence shortward of 290 nm is completely removed, due to the buildup of an ozone layer from CO_2 photolysis. However, Segura et al. (2007) note that this photochemical model neglects supply of reducing gases to the atmosphere due to volcanism and sinks of oxidic gases due to

¹A measure of reaction rate; see Section 3.4

processes involving rainout, and including either of these effects prevents the formation of an ozone layer. Geological evidence (e.g. the Tharsis plateau) indicates that young Mars had significant volcanism, which would have prevented formation of an ozone layer of the type calculated by Rontó et al. (2003).

Cnossen et al. (2007) calculate the Martian surface flux from $\sim 3.5 - 4$ Ga assuming a 5-bar CO_2 , 0.8 bar N_2 clear-sky atmosphere. They used shortwave observations of the solar analog κ^1 ceti combined with a scaled solar spectrum at longer wavelengths as their top-of-atmosphere (TOA) solar input. To calculate radiative transfer, they partition the atmosphere into 40 layers. They compute absorption using the Beer-Lambert law. To account for scattering, they compute the flux scattered in each layer, assume half of it proceeds downwards and half of it proceeds upwards, and iterate this process to the surface. This approach implicitly neglects multiple scattering and assumes a surface albedo of 0, and hence tends to overestimate atmospheric attenuation of incoming radiation. Hence, Cnossen et al. (2007) report broadband suppression of the TOA flux by multiple orders of magnitude.

Our work builds on these previous efforts. Like Cockell (2000), Rontó et al. (2003), and Cnossen et al. (2007), we consider the effects of a denser CO_2 atmosphere; however, we consider a broader range of surface atmospheric pressures permitted by available constraints, ranging from $2 \times 10^{-5} - 2$ bar. We build on Cockell (2000)’s use of a monolayer two-stream approach to radiative transfer by using a multiple-layer two stream model, which consequently accounts for the effects of multiple scattering. Such a treatment is essential because of the unique radiative transfer regime unveiled in thick anoxic atmospheres (e.g. multibar CO_2 atmospheres) at UV wavelengths, characterized by the atmosphere being simultaneously optically thick and scattering-dominated. In this regime, multiple-scattering dominates and it is critical to account for its effects in order to accurately compute surface radiation environments. As a corollary, the radiative transfer treatments of Rontó et al. (2003) and Cnossen et al. (2007) are not valid in this regime².

In addition to varying levels of CO_2 , our work also explores the impact of other potential atmospheric constituents on the surface UV environment. In particular, we focus on the effect of enhanced concentrations of volcanogenic gases (e.g., SO_2 , H_2S), which may have been present at elevated levels on the young Mars (Halevy et al. 2007; Halevy and Head 2014) and if present could have had a dramatic effect on the surface fluence (Ranjan and Sasselov 2017). We also explore the radiative impact of varying levels of dust and CO_2 and H_2O clouds in the Martian atmosphere, which may have been abundant (Wordsworth et al. 2013;

²This regime is not available on the modern Earth or Mars, due to oxitic absorption in the former and a thin atmosphere in the latter.

Halevy and Head 2014). Finally, previous workers reported the surface flux. However, as pointed out by other workers, while the flux is the relevant quantity when computing energy deposition, when computing molecular reaction rates the spherically integrated intensity, or actinic flux, is the more relevant quantity (Madronich 1987; Kylling et al. 1995). For a particle lying at the planet surface, fluence below the horizon is blocked by the surface. Therefore, we report instead the integral of the intensity field at the planet surface over the hemisphere defined by elevations > 0 (i.e. that part of the sky not blocked by the planet surface). We term this quantity the *surface radiance*. For more details, see Ranjan and Sasselov (2017).

3. Methods

In this section, we describe the methods used to calculate the surface UV environment of early Mars. All software associated with this project is available for validation and extension at <https://github.com/sukritranjan/ranjanwordsworthsasselov2016>.

3.1. Radiative Transfer Model

We use a multilayer two-stream approximation to compute the 1D radiative transfer of UV light through the early Martian atmosphere. Our code is based on the radiative transfer model of Ranjan and Sasselov (2017). In brief, we follow the two-stream treatment of Toon et al. (1989), and we use Gaussian (single) quadrature to connect the diffuse intensity to the diffuse flux, since Toon et al. (1989) find Gaussian quadrature closure to be more reliable than Eddington or hemispheric mean closure at short (solar) wavelengths. We include absorption and scattering due to N_2 , CO_2 , H_2O , CH_4 , O_2 , O_3 , SO_2 , and H_2S . For reasons of numerical stability, we assign a ceiling on the per-layer single-scattering albedo ω_0 of $1 - 10^{-12}$. In Ranjan and Sasselov (2017), we included thermal emission from the atmosphere and surface, to enable application of our code to situations where planetary UV emission might be important. Early Mars is not such a case, so here we omit these features.

Our model requires the user to specify the partition of the atmosphere into homogenous layers, and to provide the temperature, pressure, and composition (gaseous molar concentrations) as a function of altitude. Section 3.2 describes our calculation of these quantities. Our model also requires the user to specify the wavelength bins over which the radiative transfer is to be computed; all spectral parameters are integrated over these wavelength bins using linear interpolation in conjunction with numerical quadrature. The user also must specify

the solar zenith angle (SZA) and albedo. The albedo may be specified as either a fixed value (e.g. Rugheimer et al. 2015), or as a wavelength- and SZA-dependent user-determined mix of the albedos corresponding to different terrestrial physical surface media (new snow, old snow, desert, tundra, ocean).

We take the top-of-atmosphere (TOA) flux to be the solar flux at 3.9 Ga, computed at 0.1 nm resolution from the model of Claire et al. (2012) and scaled to the Martian semimajor axis of 1.524 AU. We choose 3.9 Ga for the prebiotically-relevant era 1) because of evidence for at least transient liquid water on Mars around this time (Bristow et al. 2015; Grotzinger et al. 2015; Wordsworth 2016), 2) it postdates the potentially-sterilizing Late Heavy Bombardment (Maher and Stevenson 1988; Sleep et al. 1989), and 3) it predates the bulk of the evidence for the earliest terrestrial life (see Ranjan and Sasselov 2016 and sources therein). If one hypothesizes terrestrial abiogenesis was aided by transfer of prebiotically relevant compounds from Mars (Benner 2013; Gollihar et al. 2014; Benner et al. 2015), then the synthesis of these molecules and their transfer must have occurred concomitantly with the origin of life on Earth. We note that, unlike the XUV, solar output varies only modestly (within a factor of 2) from 3.5-4.1 Ga in the > 180 nm wavelength range unshielded by atmospheric CO_2 or H_2O . Therefore, our results are insensitive to the precise choice of epoch for abiogenesis.

In Ranjan and Sasselov (2017), we did not include scattering and absorption due to atmospheric particulates. However, clouds have been suggested to play a major role in Martian paleoclimate (Forget and Pierrehumbert 1997; Colaprete and Toon 2003; Wordsworth et al. 2013). Therefore, we updated our model to allow the user to emplace CO_2 and H_2O cloud decks of user-specified optical depth (at 500 nm) in the atmosphere. The cloud decks are assumed to uniformly span the atmospheric layers into which they are emplaced. Section 3.3 discusses the calculation of the particulate optical parameters (per-particle cross-section σ , asymmetry parameter g , and ω_0). We use delta-scaling with Henyey-Greenstein closure (Joseph et al. 1976) to correct for the effects of highly forward-peaked particulate scattering phase functions.

The fundamental output of our code is the surface radiance as a function of wavelength. The surface radiance is the integral of the intensity field at the planet surface over the unit hemisphere defined by elevations greater than zero, i.e. the intensity field integrated over all parts of the sky not blocked by the planet surface. As we argue in Ranjan and Sasselov (2017), this is the relevant quantity for calculating reaction rates of molecules at planet surfaces (as compared to the actinic fluxes for molecules suspended in the atmosphere, see Madronich 1987). In the two-stream formalism, this quantity is

$$I_{surf} = F_N^\downarrow / \mu_1 + F_N^{dir} / \mu_0,$$

where F_N^\downarrow is the downward diffuse flux at the planet surface, F_N^{dir} is the direct flux at the planet surface, and $\mu_0 = \cos(SZA)$ is the cosine of the solar zenith angle. In Gaussian quadrature for the $n = 1$ (two-stream) case, $\mu_1 = 1/\sqrt{3}$ (Toon et al. 1989); it can be interpreted as the effective zenith angle for the diffuse flux.

3.2. Atmospheric Profile

We assume a CO₂-dominated Martian atmosphere at 3.9 Ga. We take the atmosphere to be fully saturated with H₂O. Typical calculations of Noachian climate call for steady-state local surface temperatures of $T_0 \lesssim 273\text{K}$ across the planetary surface, and more typically $T_0 \sim 210\text{--}250\text{K}$ (Forget et al. 2013; Wordsworth et al. 2013). Both one- and three-dimensional calculations of Noachian climate produce global mean surface temperatures of 240 K or less (Forget et al. 2013; Wordsworth et al. 2013; Ramirez et al. 2014). At such cold temperatures, the H₂O saturation pressure is very low, and H₂O is a trace gas in the atmosphere. Therefore, we approximate the thermodynamic properties of the Martian atmosphere by the thermodynamic properties of CO₂. We take $c_p = c_{p,CO_2}$ and $R = R_{CO_2}$, where c_p and R are the heat capacity at constant pressure and the specific gas constant respectively. We assume the heat capacity to be constant, with $c_p = c_p(T_0)$, where T_0 is the surface temperature. We calculate $c_p = c_{p,CO_2}$ from the Shomate relation, taking the coefficients from Pierrehumbert (2010, page 115). We tested the effects of permitting the heat capacity to vary with temperature, and found minimal impact on our results.

Martian paleoclimate models have been proposed that invoke effects like enhanced volcanism (Halevy and Head 2014) and high H₂ abundance (Ramirez et al. 2014) to argue for global mean temperatures in excess of 273K. However, these models also require pCO₂ in excess of 1 bar, meaning that H₂O remains a trace atmospheric constituent. Regardless, our results are insensitive to the precise thermal properties of the atmosphere because of the modest variation of the absorption cross-sections of the gases in our model with temperature at UV wavelengths.

For a given surface pressure, surface temperature (P_0, T_0), we let the temperature decrease as a dry adiabat until it reaches the CO₂ saturation temperature, at which point it follows the CO₂ saturation curve. We use the empirical saturation curve of Fanale et al. (1982), as in Wordsworth et al. (2013). To avoid the need for a full radiative-convective climate model, which is tangential to our objectives in this paper, we assume a stratosphere starting at 0.1 bar, following the observation of Robinson and Catling (2014) that atmospheres dominated by triatomic gases tend to become optically thin and hence radiatively dominated around that pressure. We follow other workers (e.g. Kasting 1991; Hu et al. 2012;

Halevy and Head 2014) assuming the stratosphere to be isothermal; we conduct sensitivity studies demonstrating our results are not sensitive to this assumption.

To calculate the H₂O saturation pressure, we use the empirical formulation of Wagner et al. (1994) via Wagner and Pruß (2002) for the vapor pressure of water overlying a solid reservoir (as would be the case for $T_0 < 273$ K). We assume the atmosphere to be fully saturated in H₂O until the tropopause, and we assumed the molar concentration of water in the stratosphere to be equal to its concentration at the tropopause throughout.

Our model requires temperature, pressure, and molar concentrations as functions of altitude. To obtain a mapping between pressure and altitude, we approximate the atmosphere as a series of 1000 layers, each individually isothermal, evenly spanning $P_0 - P_0 \times \exp(-10)$. We then use the equation for an isothermal atmosphere in hydrostatic equilibrium,

$$P(z)/P(z_0) = \exp(-(z - z_0)/H),$$

to calculate the change in altitude across each pressure layer, and sum to obtain a mapping between z and P . Here, P is pressure, z is the altitude of the layer top, z_0 is the altitude of the layer bottom, and $H = kT/(\mu g)$ is the scale height of the layer, with T being the layer temperature, μ the mean molecular weight of the atmospheric layer, and g the acceleration due to Martian gravity. We also considered numerically integrating the hydrostatic equilibrium equation,

$$dP/dz = -\rho g,$$

where the density $\rho = \mu P/(kT)$ for an ideal gas, directly to obtain $z(P)$. We found this approach to agree within 1%; we consequently elected to use the simpler isothermal partition approach for our calculation. Appendix A presents sample atmospheric profiles derived using our methods.

3.3. Particulate Optical Parameters

In this section, we discuss our calculation of the optical parameters (σ , ω_0 , and g) associated with interaction of radiation with the CO₂ and H₂O ice particles that constitute clouds.

We approximate the particles as spherical, and compute their optical parameters using Mie theory at 0.1 nm resolution, following the treatment outlined in Hansen and Travis (1974). At each wavelength, we compute ω_0 , g , and the scattering efficiency Q_s . We numerically integrate these parameters over a log normal size distribution with effective radius r_{eff} and effective variance v_{eff} , weighted by $\pi r^2 n(r)$, where r is the particle radius and $n(r)$

is the size distribution, and demand a precision of 1% in the distribution-averaged mean values. We obtain the per-particle total extinction cross-section by

$$\sigma = (\overline{Q_s}/\overline{\omega_0})G,$$

where $\overline{Q_s}$ is the distribution-averaged mean value of Q_s , $\overline{\omega_0}$ is the distribution-averaged mean value of ω_0 , and

$$G = \int_{r_1}^{r_2} \pi r^2 n(r) dr$$

is the "geometric cross-sectional area of particles per unit volume" (Hansen and Travis 1974) computed at 1 ppm precision. For our numerical integral, we integrated from $r_1 = r_{eff}10^{-10v_{eff}}$ to $r_2 = r_{eff}10^{4v_{eff}}$; we found $n(r) < 10^{-4}$ beyond these limits.

We take the index of refraction for H₂O ice from the compendium of Warren and Brandt (2008)³. We take the index of refraction for CO₂ ice from the compendium given in Pierrehumbert (2010)⁴. This compendium was formed by G. Hansen by subjecting the absorption spectra of Hansen (1997) and Hansen (2005) to Kramers-Kronig analysis to obtain self-consistent spectra of real and imaginary indices of refraction (S. Warren, private communication). We take the index of refraction for Martian dust from Wolff et al. (2009)⁵. The data of Wolff et al. (2009) truncate at 263 nm. Measurements of the imaginary index of refraction down to 194 nm are available from Pang and Ajello (1977). We adopt the values of Pang and Ajello (1977) for wavelengths < 263 nm. Zurek (1978) present a compendia of the real index of refraction of Martian dust. Their study indicates that the index of refraction changes by only ~ 0.1 from $\sim 200 - 263$ nm. Their values at 263 nm are 0.4 higher than Wolff et al. (2009); to avoid a discontinuity, we subtract 0.4 from the real indices of refraction of Zurek (1978).

Figure 1 presents the CO₂ and H₂O ice optical parameters as a function of wavelength for size distributions with $v_{eff} = 0.1$ and $r_{eff} = 1, 10, 100$ microns. Previous work has assumed CO₂ cloud particle sizes to be in the 1-100 μm range (e.g., Forget and Pierrehumbert 1997). Microphysical modelling by Colaprete and Toon (2003) suggests that primitive Martian CO₂ clouds may have been characterized by large particle sizes, as high as $r_{eff} = 100\mu\text{m}$. The optical properties of CO₂ and H₂O ice particles for $r_{eff} \geq 10\mu\text{m}$ insensitive to r_{eff} ; we

³accessed via http://www.atmos.washington.edu/ice_optical_constants

⁴accessed via <http://geosci.uchicago.edu/~rtp1/PrinciplesPlanetaryClimate/Data/WorkbookDatasets/Chapter5Data/co2i4a.rfi.txt>

⁵accessed via http://spacescience.arc.nasa.gov/mars-climate-modeling-group/documents/Dust_Refractive_Indicies.txt

attribute this to size parameter $x = 2\pi r_{eff}/\lambda$ being large in this regime, meaning such particles approach the large-particle limit. ($x > 12$ for $r_{eff} \geq 10\mu\text{m}$ and $\lambda \leq 500\text{ nm}$). For wavelengths satisfying $195 < \lambda < 500\text{ nm}$, CO_2 and H_2O ice are characterized by $\omega_0 \approx 1$. This means that CO_2 and H_2O clouds do not significantly absorb at wavelengths unshielded by H_2O ($< 198\text{ nm}$) or CO_2 ($< 204\text{ nm}$). By contrast, dust absorbs across $100 - 500\text{ nm}$, meaning dust particles can supply absorption at wavelengths not shielded by CO_2 or H_2O .

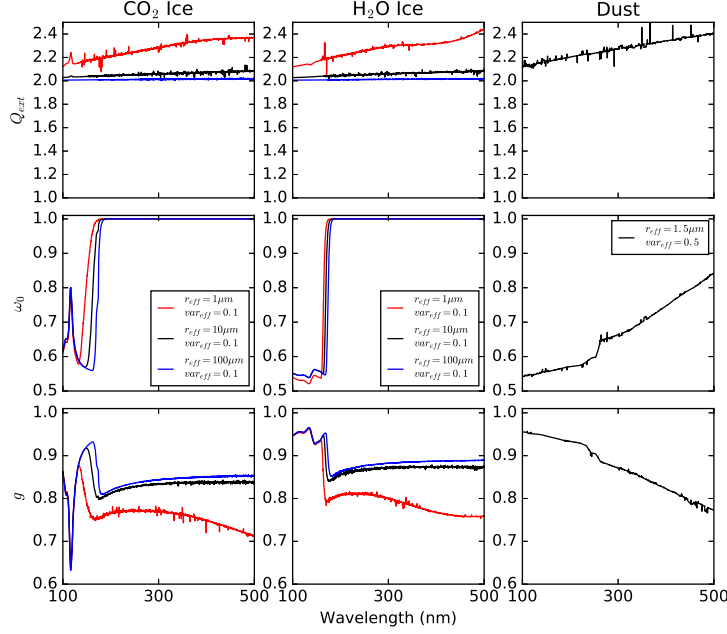


Fig. 1.— Scattering efficiency Q_{ext} , single-scattering albedo ω_0 , and asymmetry parameter g as a function of wavelength for CO_2 ice, H_2O ice, and modern Martian dust, integrated over the specified log-normal size distributions.

3.4. Action Spectra and Calculation of Dose Rates

To quantify the impact of different surface UV radiation environments on prebiotic chemistry, we follow the approach of Cockell (1999), Rontó et al. (2003), and Rugheimer et al. (2015) in computing Biologically Effective Dose rates (BEDs). Specifically, we compute

$$D = \left(\int_{\lambda_0}^{\lambda_1} d\lambda \mathcal{A}(\lambda) I_{surf}(\lambda) \right),$$

where $\mathcal{A}(\lambda)$ is an action spectrum, λ_0 and λ_1 are the limits over which $\mathcal{A}(\lambda)$ is defined, and $I_{surf}(\lambda)$ is the UV surface radiance. An action spectrum parametrizes the relative impact

of radiation on a given photoprocess as a function of wavelength, with a higher value of \mathcal{A} meaning that a higher fraction of the incident photons are being used in the photoprocess. Hence, D is proportional to the reaction rate rate of a given photoprocess for a single molecule at the surface of a planet.

As D is a relative measure of reaction rate, a normalization is required to assign a physical interpretation to its value. In this paper, we report

$$\bar{D} = D/D_{\oplus},$$

where D_{\oplus} is the dose rate on 3.9 Ga Earth. The atmospheric model for 3.9 Ga Earth is taken from Rugheimer et al. (2015), who use a 1D coupled climate-photochemistry model to compute the atmospheric profile (T, P, composition) for the Earth at 3.9 Ga, assuming modern abiotic outgassing rates and a background atmosphere of 0.9 bar N_2 , 0.1 bar CO_2 , with $\text{SZA}=60^\circ$ and $A = 0.2$. Consequently, $\bar{D} > 1$ means that the photoprocess is proceeding faster on the Martian surface under the specified atmosphere than it would on the surface of the Rugheimer et al. (2015) fiducial Earth. Note this normalization is different from what we chose in Ranjan and Sasselov (2017), because here we are trying to assess how Mars compares to the Earth as a venue for prebiotic chemistry.

Previous workers used action spectra of UV stress on modern biology (e.g. the DNA inactivation action spectrum) (Cockell 2000, 2002; Cnossen et al. 2007; Rugheimer et al. 2015) as a gauge of the level of stress imposed by UV fluence on the prebiotic environment. However, these action spectra are based on modern life. Modern organisms have evolved sophisticated methods to deal with environmental stress, including UV exposure, that would not have been available to the first life. Further, this approach presupposes that UV light is solely a stressor, and ignores its potential role as a eustressor for abiogenesis. In this work, we follow the reasoning of our previous efforts in Ranjan and Sasselov (2017) in formulating action spectra corresponding to simple photoreactions that are expected to have played major roles in prebiotic chemistry. We consider two reactions: a stressor process, to capture the stress UV light places on nascent biology, and an eustressor process, to capture the role of UV light in promoting prebiotic chemistry. A detailed description of these processes and their corresponding action spectra is given in Ranjan and Sasselov (2017); a brief outline is presented below.

3.4.1. *Stressor Process: Cleavage of N-Glycosidic Bond of UMP*

For our stressor process, we chose the cleavage of the N-glycosidic bond in the RNA monomer uridine monophosphate (UMP). UV radiation can cleave the N-glycosidic bond

which joins the sugar to the nucleobase (Gurzadyan and Görner 1994), irreversibly destroying this molecule. Hence, this process represents a stressor to abiogenesis.

The action spectrum is equal to the product of the absorption spectrum (fraction of incident photons absorbed) and the quantum yield curve (QY, fraction of absorbed photons that lead to the photoreaction). We take our UMP absorption spectrum from the work of (Voet et al. 1963) (pH=7.6). Detailed spectral measurements of the QY of glycosidic bond cleavage have not been obtained. However, Gurzadyan and Görner (1994) found the QY of N-glycosidic bond cleavage in UMP in neutral aqueous solution saturated with Ar (i.e. anoxic) to be 4.3×10^{-3} at 193 nm and $(2 - 3) \times 10^{-5}$ for 254 nm. We therefore represent the QY curve as a step function with value 4.3×10^{-3} for $\lambda \leq \lambda_0$ and 2.5×10^{-5} for $\lambda > \lambda_0$. We consider λ_0 values of 193 and 254 nm, corresponding to the empirical limits from Gurzadyan and Görner (1994). We also consider $\lambda_0 = 230$ nm, which corresponds to the end of the broad absorption feature centered near 260 nm corresponding to the $\pi - \pi^*$ transition and also to the transition to irreversible decomposition suggested by Sinsheimer and Hastings (1949). As shorthand, we refer to this photoprocess under the assumption that $\lambda_0 = X$ nm by UMP-X. Figure 2 presents these action spectra.

The absorption spectra of the other RNA monomers are structurally similar to UMP (Voet et al. 1963), and the quantum yield of N-glycosidic bond cleavage in adenosine monophosphate (AMP) increases at short wavelengths like UMP’s does (Gurzadyan and Görner 1994), leading us to argue that action spectra for N-glycosidic bond cleavage of the other RNA monomers should be broadly similar to that for UMP. Therefore, results derived using the action spectrum for UMP N-glycosidic bond cleavage should be broadly applicable to the other RNA monomers: if a UV environment is destructive for UMP, it should be bad for the other RNA monomers, and hence for abiogenesis in the RNA world hypothesis, as well.

3.4.2. *Eustressor Process: Production of Aquated Electrons from Photoionization of Cyanocuprate*

For our eustressor process, we choose the production of aquated electrons from the irradiation of a tricyanocuprate (CuCN_3^{2-}) complex. We chose this process because it underlies the selective 2- and 3-carbon sugar (glycolaldehyde and glyceraldehyde) synthesis pathway of Ritson and Sutherland (2012), which is the best candidate proposed so far for a selective prebiotic synthesis of these sugars. These sugars are required for the synthesis of RNA, and hence abiogenesis in the RNA world hypothesis. This process is also important to the prebiotic reaction network of Patel et al. (2015). More generally, aquated electrons are useful for a broad range of reductive prebiotic chemistry, e.g., the reduction of nitriles to amines, alde-

hydres to hydroxyls, and hydroxyls to alkyls⁶. Therefore, this process represents a eustressor to abiogenesis. While other UV-sensitive processes conducive to abiogenesis doubtless exist, we argue this process is of particular interest because of its unique role in the most promising plausibly prebiotic pathways to the RNA monomers.

We again form the action spectrum by multiplying the absorption spectrum and the quantum yield curve. We take the cyanocuprate absorption spectrum from the work of Magnani (2015), via Ranjan and Sasselov (2016). The spectral QY of aquated electron production from cyanocuprate irradiation is not known. However, Horváth et al. (1984) measure a QY of 0.06 for this process at 254 nm. Following Ritson and Sutherland (2012)’s hypothesis that photoionization of the complex drives aquated electron production, we assume the QY to be characterized by a step function with value 0.06 for $\lambda \leq \lambda_0$ and 0 otherwise. We empirically know $\lambda_0 \geq 254$ nm. To explore a range of λ_0 , we consider $\lambda_0 = 254$ nm and $\lambda_0 = 300$ nm. As shorthand, we refer to this photoprocess under the assumption that $\lambda_0 = Y$ nm by CuCN3-Y. Figure 2 presents these action spectra.

Action spectra typically encode information about relative, not absolute, reaction rates. Consequently, they are generally arbitrarily normalized to 1 at some wavelength (see, e.g., Cockell 1999 and Rugheimer et al. 2015). We normalize these spectra to 1 at 190 nm.

⁶J. Szostak, private communication, 2/5/16

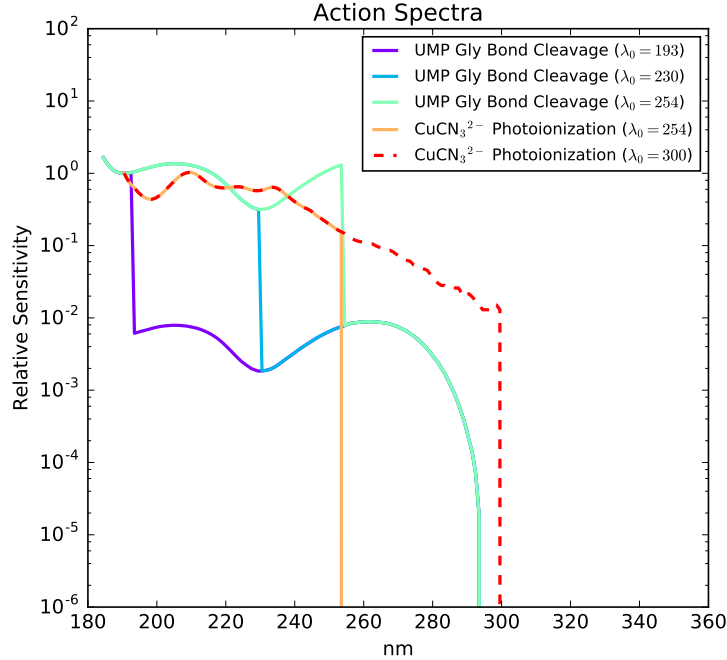


Fig. 2.— Action spectra for photolysis of UMP— λ_0 and photoionization of CuCN₃— λ_0 , assuming a step-function form to the QE for both processes with step at λ_0 . The spectra are arbitrarily normalized to 1 at 190 nm.

4. Results

4.1. Clear-Sky H₂O-CO₂ Atmospheres

We evaluated the UV surface radiance for a range of ($p\text{CO}_2$, T_0) for pure H₂O-CO₂ atmospheres in the clear-sky case (no clouds, dust or other particulates). We considered $p\text{CO}_2 = 0.02 - 2$ bar, corresponding to the range of surface pressure for which Wordsworth et al. 2013 reported at least transient local temperatures above 273 K, and $T_0 = 210 - 300$ K. We took an SZA of 0, corresponding to noon at equatorial latitudes. We took the surface albedo to correspond to desert (diffuse albedo of 0.22); we adopted this albedo because 1) young Mars is thought to have been dry and desertlike in conventional climate models, and 2) the desert diffuse albedo corresponds roughly to modern Mars’s surface albedo (e.g., Kasting 1991). We note that variations in surface albedo and SZA can drive variations in the spectral surface radiance of up to a factor of ~ 20 , and overall variations in prebiotically-relevant reaction rates of a factor of $\gtrsim 10$ (Ranjan and Sasselov 2017). These surface radiances are shown in Figure 3.

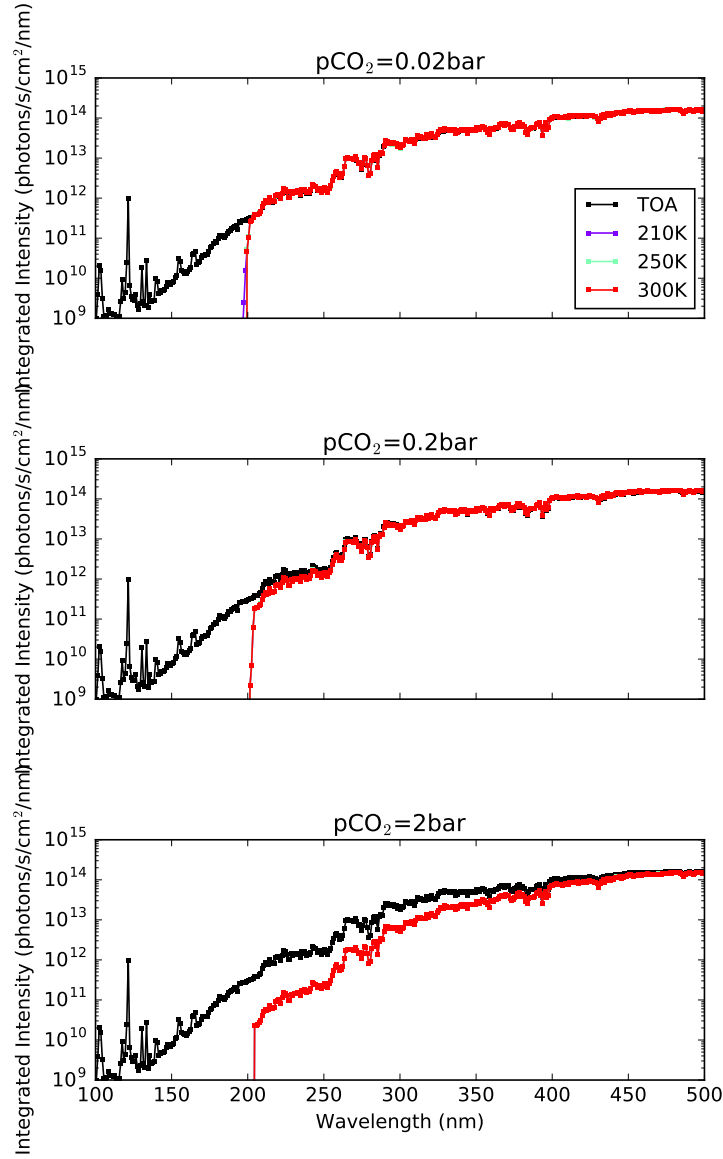


Fig. 3.— Surface radiance as a function of wavelength for varying pCO₂ and T_0 , for SZA=0 and albedo corresponding to desert. Also plotted for scale is the TOA solar flux. The surface radiance is insensitive to atmospheric and surface temperature.

In the scattering regime ($\lambda > 204$ nm), our surface radiances fall off only slowly with pCO₂. This is a consequence of random walk statistics in the context of multiple scattering: transmission through purely scattering media go as $1/\tau$ (see, e.g., Bohren 1987 for a discussion with application to clouds). This result stands in contrast to the calculations of Cnossen et al. (2007) and Rontó et al. (2003), who ignore multiple scattering in their ra-

diative transfer treatments, and illustrates the importance of self-consistently including this phenomenon when considering dense, highly scattering atmospheres.

We find our surface radiance calculations to be insensitive to T_0 . This is because 1) the total atmospheric column is set by P_0 and independent of T_0 , 2) the rapid increase of CO_2 cross-sections for $\lambda < 204$ nm, which means that the atmosphere rapidly becomes optically thick in the UV, and 3) increased water vapor abundance with increasing T_0 does not drive an increase in opacity because water vapor absorption is degenerate with CO_2 absorption in the UV (Ranjan and Sasselov 2017).

We considered the hypothesis that including the effect of variations in CO_2 cross-section with temperature might impact our results. We followed the approach of Hu et al. (2012) in interpolating between cold (~ 195 K) and room-temperature datasets for CO_2 absorption to estimate the effects of temperature dependence on CO_2 cross-section. We used the dataset of Stark et al. (2007) from 106.5-118.7 nm, Yoshino et al. (1996) from 118.7-163 nm, and Parkinson et al. (2003) from 163-192.5 nm. We did not find cold-temperature cross-sections for CO_2 at longer wavelengths. We found our results were not altered by including temperature-dependence of CO_2 cross-sections for $p\text{CO}_2 = 0.02 - 2$ bar, because the CO_2 UV absorption is already saturated by 192.5 nm, where our temperature dependence kicks in. We considered lower values of $p\text{CO}_2 = 2 \times 10^{-3} - 2 \times 10^{-5}$ bar (below PAL), where the CO_2 absorption does not saturate until wavelengths shorter than 192.5 nm. Even in the low $p\text{CO}_2$ case, including temperature-dependence only changed the onsite of CO_2 absorption saturation by 1 – 2 nm. We attribute this to the rapidity of the rise in CO_2 absorption cross section with decreasing wavelength for $\lambda \lesssim 204$ nm. We conclude that even including the effects of temperature on CO_2 UV cross-section, the UV surface fluence is insensitive to T_0 . We consequently elected to ignore the temperature dependence of CO_2 cross-sections in the remainder of this study.

Figure 4 presents the surface radiances in the $p\text{CO}_2 = 2 \times 10^{-5}$ bar cases, calculated for $\text{SZA}=0$, A corresponding to desert, and $T_0 = T_{eq} \approx 200\text{K}$, with and without CO_2 cross-sections included. Such low atmospheric pressures have been suggested based on atmospheric escape arguments (Tian et al. 2009), followed by a buildup of the atmosphere after escape rates subsided with shortwave solar output. In such a case, aqueous prebiotic chemistry could only have proceeded in environments kept warm by non-climatological means, e.g. geothermal reservoirs. Even for such low $p\text{CO}_2$, EUV fluence shortward of 185 nm is shielded out by atmospheric CO_2 .

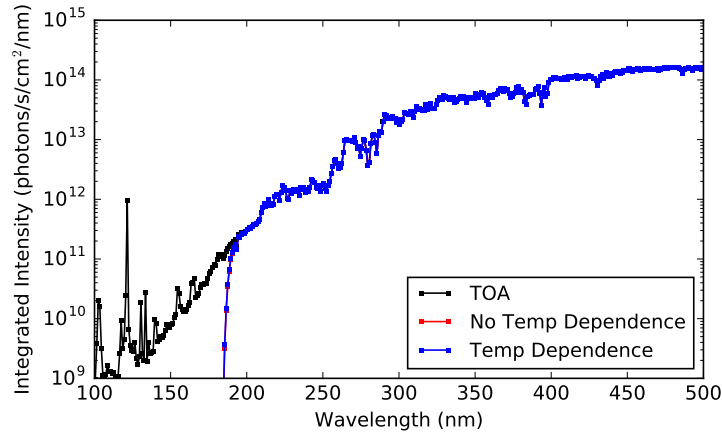


Fig. 4.— Surface radiance as a function of wavelength for $p\text{CO}_2 = 2 \times 10^{-5}$ bar, $T_0 = 200\text{K}$, $\text{SZA}=0$, A corresponding to desert, with and without temperature dependence of the CO_2 cross-sections included. Also plotted for scale is the TOA solar flux. The surface radiance is insensitive to inclusion of temperature dependence of the CO_2 cross-sections, even for very low $p\text{CO}_2$.

4.2. Effect of CO_2 and H_2O Clouds

We considered the effect of CO_2 and H_2O clouds in a CO_2 - H_2O atmosphere. Such clouds have been detected on modern Mars (see, e.g., Vincendon et al. 2011), and GCM results suggest they should have been present on early Mars as well (Wordsworth et al. 2013). Figure 5 presents the UV surface fluence for a 0.02-bar CO_2 - H_2O atmosphere with H_2O and CO_2 cloud decks of varying optical depths emplaced in the atmosphere. This low surface pressure is chosen in order to isolate the effects of the clouds as opposed to atmospheric CO_2 . The surface albedo corresponds to desert, and $\text{SZA}=0$. The optical depths are specified at 500 nm. The H_2O and CO_2 cloud decks are emplaced from 3-4 km and 20-21 km of altitude, respectively, corresponding approximately to the altitudes of peak cloud formation identified in Wordsworth et al. (2013). For both types of clouds, we varied the cloud deck altitudes between 0.5-60.5 km, and found the surface fluence to be insensitive to the cloud deck altitude. We also experimented with partitioning the clouds into two decks, and found the surface fluence to be insensitive to the partition.

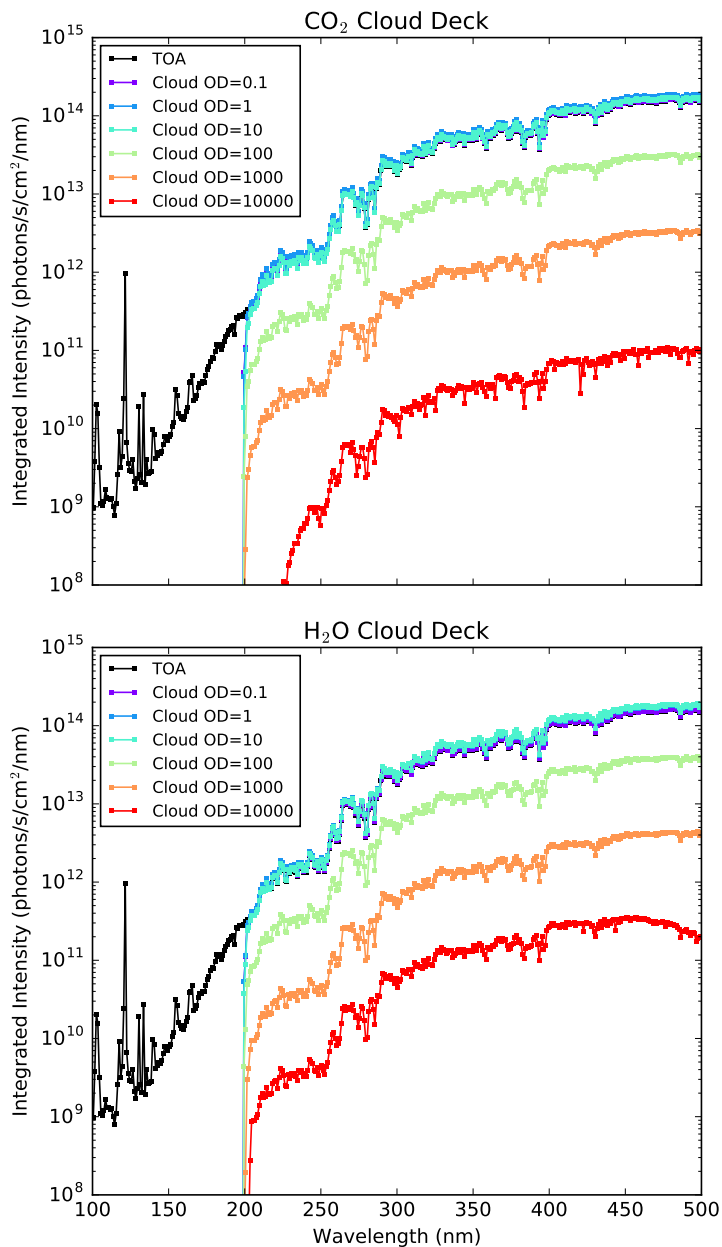


Fig. 5.— Surface radiance as a function of wavelength for $p\text{CO}_2 = 0.02$ bar, $T_0 = 250\text{K}$, $\text{SZA}=0$, A corresponding to desert, and CO_2 and H_2O cloud decks of varying thicknesses inserted from 20-21 and 3-4 km respectively. Also plotted for scale is the TOA solar flux.

CO_2 and H_2O ice clouds have similar impact on the surface fluence. This is because both types of ice have similar optical parameters for $195 < \lambda < 500$ nm and $r_{eff} \geq 1\mu\text{m}$.

The $\lambda < 195$ nm regime, where they have different optical parameters, is shielded out by gaseous CO₂ absorption.

CO₂ and H₂O ice particles are pure scatterers for $195 < \lambda < 500$ nm and $r_{eff} \geq 1\mu\text{m}$. Consequently, it is unsurprising that surface fluence falls off only slowly with increasing optical depth. In fact, the transmission of a purely scattering cloud layer varies as $\sim 1/\tau^*$, where τ^* is the delta-scaled optical depth of the cloud layer (Bohren 1987). This is a consequence of the random-walk nature of radiative transfer in the optically-thick purely-scattering limit.

The particle size r_{eff} can have an impact on surface radiance. For $r_{eff} = 1\mu\text{m}$, the surface fluence at 500 nm is $\sim 40\%$ lower compared to $r_{eff} = 100\mu\text{m}$ (*A* corresponding to desert, SZA=0). This is because as r_{eff} decreases in this regime, so does g , meaning that the rescaled optical depth in the delta-scaling formalism $\tau^* = \tau \times (1 - g^2)$ is higher for small particles than large particles.

Suppressing surface radiance to 10% or less of TOA flux requires cloud optical depths of $\gtrsim 100$. This is comparable to the optical depth of a terrestrial thunderstorm (Mayer et al. 1998). We can compute the mass column of ice particle required to achieve this optical depth by

$$u = \left(\frac{\tau}{\pi r^2 Q_{ext}}\right) \left(\frac{4\pi}{3} r^3 \rho\right),$$

where ρ is the mass density of the ice, r is the ice particle radius, τ is the cloud optical depth, and Q_{ext} is the extinction efficiency. For CO₂ ice, $\rho = 1.5$ g/cm³ ⁷, $r = 10\mu\text{m}$, and approximating $Q_{ext} = 2$, we find $\tau = 100$ corresponds to $u = 1$ kg/m². Wordsworth et al. (2013) find in their 3D simulation CO₂ ice columns of up to 0.6 kg/m² in patches, suggesting CO₂ clouds may have significantly affected the surface UV environment. For water ice, taking $\rho = 0.92$ g/cm³ (Miller 2009), $r = 10\mu\text{m}$, and approximating $Q_{ext} \approx 2$, we find $\tau = 100$ corresponds to $u = 6 \times 10^{-1}$ kg/m². By contrast, Wordsworth et al. (2013) finds expected ice columns of $\lesssim 2 \times 10^{-3}$ kg/m². Consequently, barring a mechanism which can increase the H₂O cloud levels above that considered by Wordsworth et al. (2013), H₂O ice clouds by themselves are unlikely to significantly alter the surface radiance environment on early Mars.

⁷<http://terpconnect.umd.edu/~choi/MSDS/Airgas/CARBON%20DIOXIDE.pdf>

4.3. Effect of Elevated Levels of Volcanogenic Gases

So far, we have considered pure CO₂-H₂O atmospheres. However, other gases may have been present in the early Martian atmosphere. In particular, Mars at ~ 3.9 Ga was characterized by volcanic activity, which emplaced features like the Tharsis igneous province (Halevy and Head 2014). Such volcanism could have injected elevated levels of volcanogenic gases like SO₂ and H₂S into the atmosphere. SO₂ and H₂S are also strong and broad UV absorbers, and at elevated levels they can completely reshape the surface UV environment (Ranjan and Sasselov 2017). Consequently, we consider the impact of elevated levels of SO₂ and H₂S on the surface UV environment.

We consider SO₂ levels up to 2×10^{-5} bar. For scale, Halevy and Head (2014) compute that an SO₂ level of 1×10^{-5} bar in a 1 bar CO₂-dominated atmosphere requires volcanic outgassing at $100\times$ the current terrestrial outgassing. Figure 6 presents the surface radiance for varying pSO₂ and pCO₂ = 0.02–2 bar (SZA=0, A corresponding to desert, and $T_0 = 250$ K).

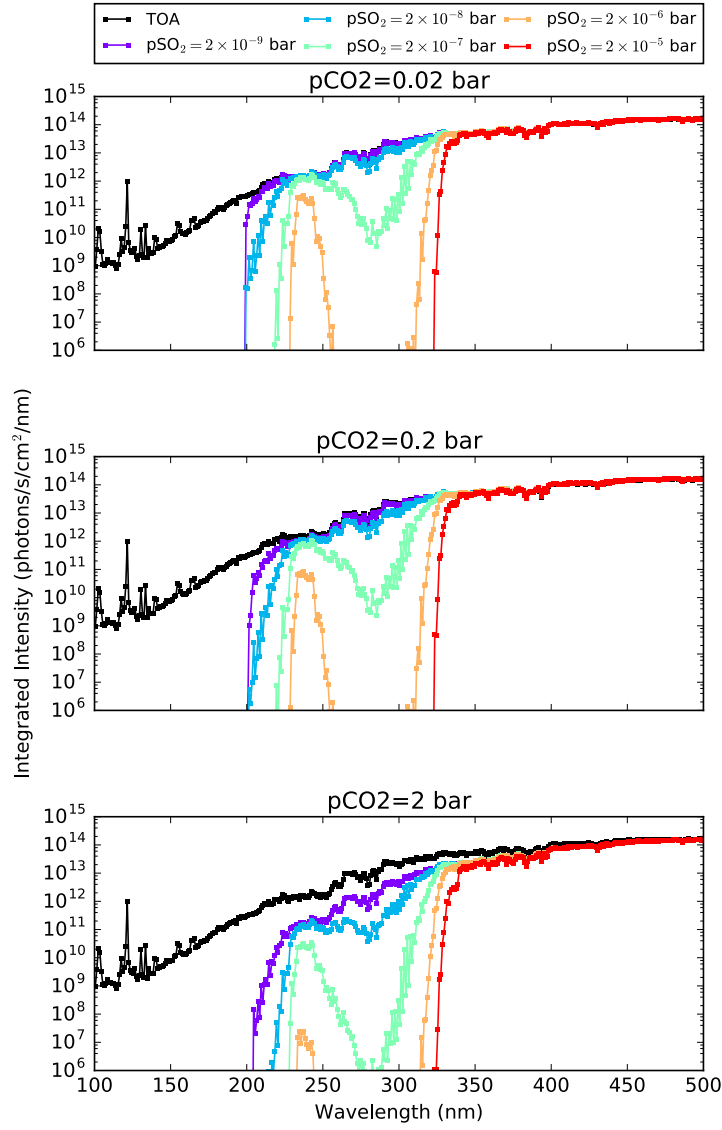


Fig. 6.— Surface radiance as a function of wavelength for $T_0 = 250\text{K}$, $\text{SZA}=0$, A corresponding to desert, $\text{pCO}_2 = 0.02 - 2 \text{ bar}$, and $\text{pSO}_2 = 2 \times 10^{-9} - 2 \times 10^{-5} \text{ bar}$. Also plotted for scale is the TOA solar flux.

Note that for the same pSO_2 , the surface radiance varies as a function of pCO_2 . This is because at high pCO_2 , the scattering optical depth of the atmosphere exceeds unity. In such a regime, the impact of trace absorbers is amplified due to higher effective path length caused by multiple scattering events (Bohren 1987). This effect has been seen in studies of UV transmittance through thick clouds on Earth as well (Mayer et al. 1998). Consequently,

the surface UV environment is a feature of both $p\text{CO}_2$ and $p\text{SO}_2$. For $p\text{SO}_2 \geq \times 10^{-5}$ bar, UV fluence < 330 nm is strongly suppressed.

H_2S is also a major volcanogenic gas that may have been emitted at rates greater than or equal to SO_2 on young Mars, based on studies of the oxidation state of Martian basalts (Herd et al. 2002; Halevy et al. 2007). While Halevy and Head (2014) do not calculate the H_2S abundance as a function of volcanic outgassing, the calculations of Hu et al. (2013) ($T_0=288\text{K}$, modern solar irradiance) suggest that $p\text{H}_2\text{S} > p\text{SO}_2$ in a CO_2 dominated atmosphere. Consequently, we also consider the impact of elevated levels of H_2S , up to $p\text{H}_2\text{S}=2 \times 10^{-4}$ bar in atmospheres with $p\text{CO}_2 = 0.02 - 2$ bar. Figure 7 presents the surface radiance calculated over this range of atmospheres ($\text{SZA}=0$, A corresponding to desert, and $T_0 = 250$ K). For $p\text{H}_2\text{S} \geq \times 10^{-4}$ bar, UV fluence < 370 nm is strongly suppressed.

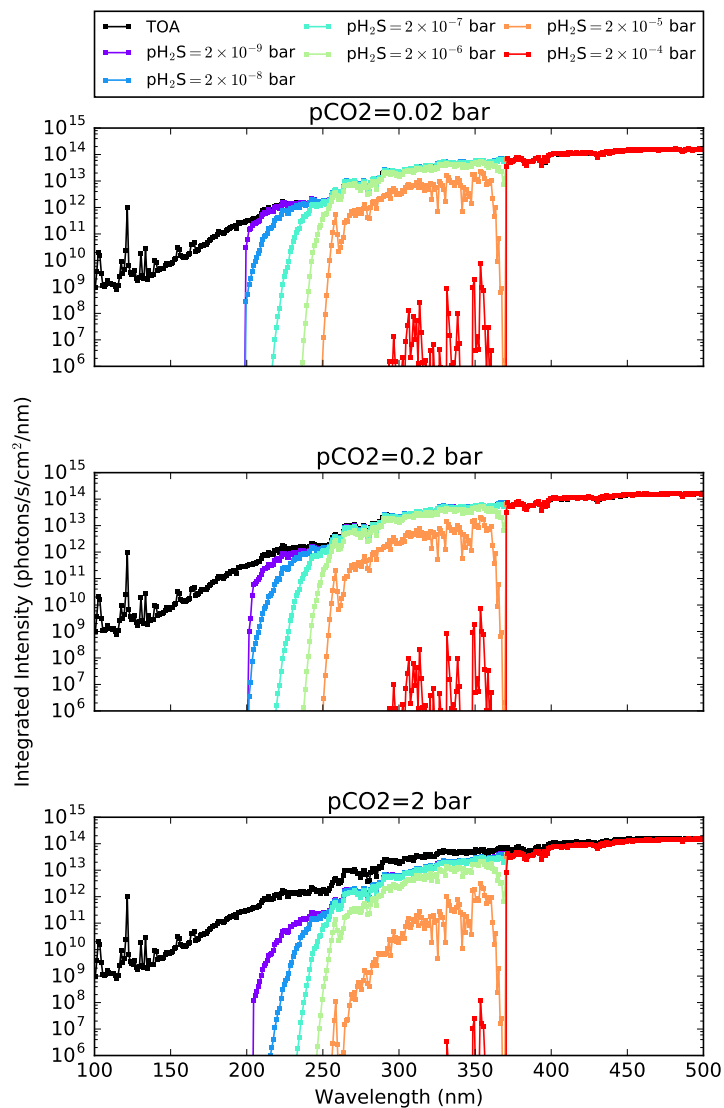


Fig. 7.— Surface radiance as a function of wavelength for $T_0 = 250\text{K}$, $\text{SZA}=0$, A corresponding to desert, $\text{pCO}_2 = 0.02 - 2$ bar, and $\text{pH}_2\text{S} = 2 \times 10^{-9} - 2 \times 10^{-4}$ bar. Also plotted for scale is the TOA solar flux.

Scattering due to thick cloud decks can also enhance absorption by trace pSO_2 and pH_2S . For $\text{pSO}_2 = 2 \times 10^{-7}$ bar and $\text{pCO}_2=0.02$ bar⁸ ($\text{SZA}=0$, A corresponding to new snow

⁸At $\text{pCO}_2=0.02$ bar, the gaseous scattering optical depth is less than unity for wavelengths longer than 204 nm, meaning that we can attribute this amplification primarily to the cloud deck (as opposed to gaseous

(near 1), $T_0 = 250$ K, $r_{eff} = 10\mu\text{m}$), inclusion of CO_2 clouds with optical depth of 1000 amplifies attenuation by a factor of 10 at 236.5 nm (optically thin in SO_2 absorption) and by a factor of 10^5 at 281.5 nm (optically thick in SO_2 absorption) compared to what one would calculate by multiplying the transmission from the SO_2 and cloud deck individually. This effect is weaker for low-albedo cases, because there are fewer passes of radiation through the atmosphere due to bouncing between the surface and cloud deck. This nonlinear variance in transmission due to multiple scattering effects illustrates the need to specify surface albedo, cloud thickness and absorber level when calculating surface radiances. Figure 8 and Figure 9 present the surface radiance at the base of a $\text{pCO}_2=0.02$ bar atmosphere with varying levels of SO_2 and H_2S respectively, with CO_2 cloud decks of optical depths 1 – 1000 emplaced from 20-21 km (SZA=0, A corresponding to desert, $T_0 = 250$ K, $r_{eff} = 10\mu\text{m}$).

scattering).

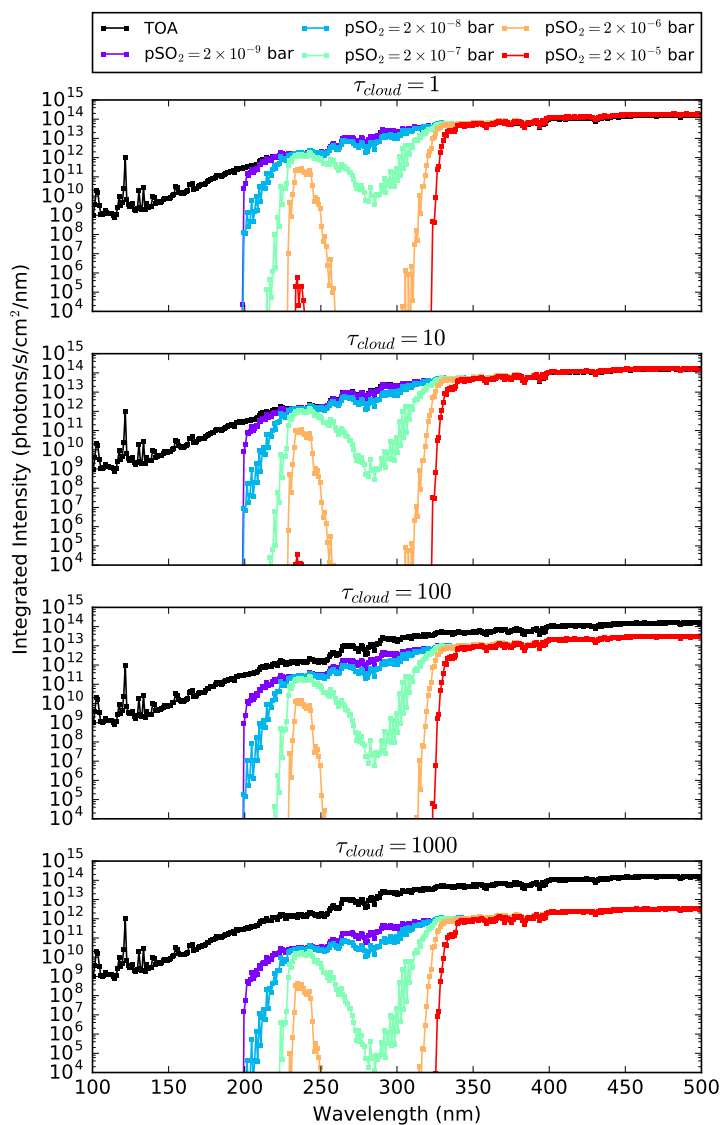


Fig. 8.— Surface radiance as a function of wavelength for $T_0 = 250\text{K}$, $\text{SZA}=0$, A corresponding to desert, $\text{pCO}_2 = 0.02$ bar, $\text{pSO}_2 = 2 \times 10^{-9} - 2 \times 10^{-5}$ bar, and CO_2 cloud decks of varying optical thickness emplaced from 20-21 km altitude. Also plotted for scale is the TOA solar flux.

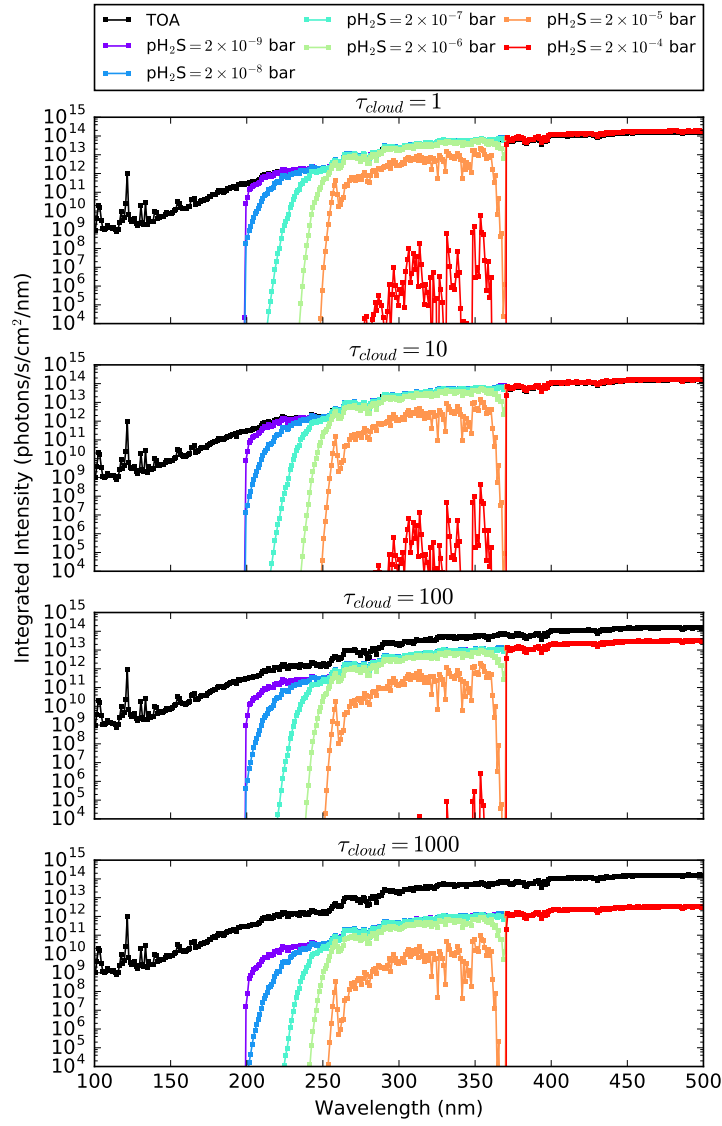


Fig. 9.— Surface radiance as a function of wavelength for $T_0 = 250\text{K}$, $\text{SZA}=0$, A corresponding to desert, $\text{pCO}_2 = 0.02$ bar, $\text{pH}_2\text{S} = 2 \times 10^{-9} - 2 \times 10^{-4}$ bar, and CO_2 cloud decks of varying optical thickness emplaced from 20-21 km altitude. Also plotted for scale is the TOA solar flux.

4.4. Effect of Dust

The atmosphere of modern Mars is dusty, with typical dust optical depths varying from $\tau_d \sim 0.2 - 2$ at solar wavelengths (Smith et al. 2002; Lemmon et al. 2015), with the higher

values achieved during global dust storms. Mars’s dryness contributes to its dustiness, through the availability of desiccated surface to supply dust and the lack of a hydrologic cycle to quickly scrub it from the atmosphere. If one assumes that Mars were similarly dry in the past, dust levels in the Martian atmosphere may have been significant. We may speculate that if the atmosphere were thicker, it could have hosted even more dust than the modern Martian atmosphere due to slower sedimentation times. However, detailed study of atmospheric dust dynamics, including analysis of how dust lofting scales with pCO₂, is required to constrain this possibility. Dust absorbs at UV wavelengths (see Figure 1), so dust could play a role similar to volcanogenic gases in scrubbing UV radiative from the UV surface environment.

We explored the impact of including dust in our calculation of surface UV fluence. We assumed that, similar to the modern Mars, the dust followed an exponential profile with scale height $H_d = 11$ km, similar to the atmospheric pressure scale height (Hoekzema et al. 2010; Mishra et al. 2016). For surface temperatures (and hence scale heights) comparable to modern Mars, this corresponds to the assumption by previous workers that the dust mixing ratio is constant in the lower atmosphere (Forget et al. 1999). Then, the dust optical depth across each atmospheric layer of width Δz is

$$C \exp[-z/H_d],$$

where z is the altitude of the layer center. The parameter

$$C = \tau_d(\exp[\Delta z/(2H_d)])(1 - \exp[-\Delta z/H_d])$$

, is chosen such that the column-integrated dust optical depth is τ_d .

Figure 10 presents the surface radiance for varying τ_d and pCO₂ = 0.02 – 2 bar (SZA=0, A corresponding to desert, and $T_0 = 250$ K). As for SO₂ and H₂S, highly scattering atmospheres amplify the impact of trace absorbers. $\tau_d = 1$ only marginally suppresses UV fluence for pCO₂ = 0.02 bar, but for pCO₂ = 2 bar shortwave fluence is suppressed due to enhanced Rayleigh scattering. In the absence of scattering amplification, $\tau_d \gtrsim 10$ is required to strongly suppress UV fluence.

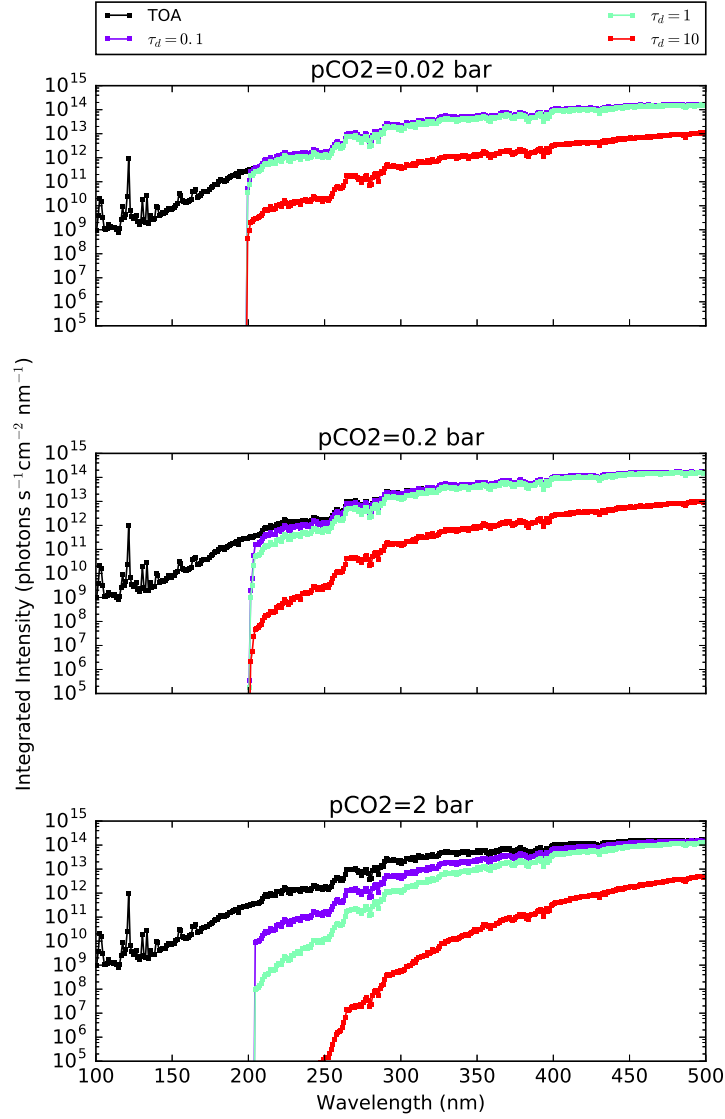


Fig. 10.— Surface radiance as a function of wavelength for $T_0 = 250\text{K}$, $\text{SZA}=0$, A corresponding to desert, $\text{pCO}_2 = 0.02 - 2$ bar, and $\tau_d = 0.1 - 10$. Also plotted for scale is the TOA solar flux.

Figure 11 presents the surface radiance at the base of a $\text{pCO}_2=0.02$ bar atmosphere with varying τ_d , with CO_2 cloud decks of optical depths 1 – 1000 emplaced from 20-21 km ($\text{SZA}=0$, A corresponding to desert, $T_0 = 250$ K, $r_{eff} = 10\mu\text{m}$). The impact of a cloud deck is less than the impact of increasing overall atmospheric pressure, because of the limited column of absorber contained within the cloud itself. If the cloud deck is extended, then the

surface fluence is reduced (for the same total cloud and dust optical depth).

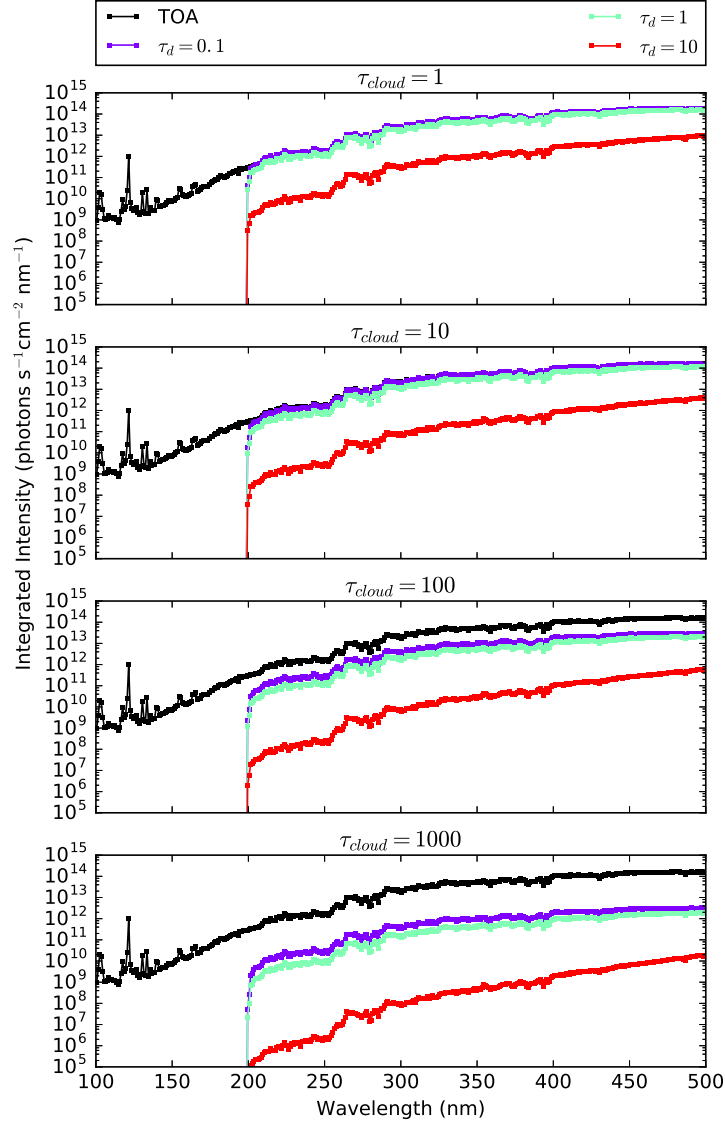


Fig. 11.— Surface radiance as a function of wavelength for $T_0 = 250K$, $SZA=0$, A corresponding to desert, $pCO_2 = 0.02$ bar, $\tau_d = 0.1 - 10$, and CO_2 cloud decks of varying optical thickness emplaced from 20-21 km altitude. Also plotted for scale is the TOA solar flux.

5. Discussion

5.1. CO₂-H₂O Atmosphere

Normative CO₂-H₂O climate models predict the steady-state early Martian climate to have been cold, with global mean temperatures below freezing (Forget et al. 2013; Wordsworth et al. 2013; Wordsworth et al. 2015). In this scenario, aqueous prebiotic chemistry would proceed in meltwater pools, which could have occurred transiently during midday due to the diurnal cycle, during summer during a seasonal cycle, or a combination of both. Aqueous prebiotic chemistry could also have proceeded in geothermally heated pools, which may have been abundant during the more volcanically active Noachian.

Figure 12 presents the dose rates \bar{D}_i corresponding to irradiation of prebiotically relevant molecules through a clear-sky CO₂-H₂O atmosphere with SZA=0 and A corresponding to desert. The dose rates \bar{D}_i decline by only an order of magnitude across 5 orders of magnitude of pCO₂ ≤ 2 bar, meaning that the prebiotic photochemistry dose rates are only weakly sensitive to pCO₂ across this range. \bar{D}_i is within an order of magnitude of unity across this range, meaning that the Martian dose rates are comparable to the terrestrial rates. This is consistent with the results of Cockell (2000), who found that UV stress as measured by DNA damage were comparable for 3.5 Ga Earth and Mars.

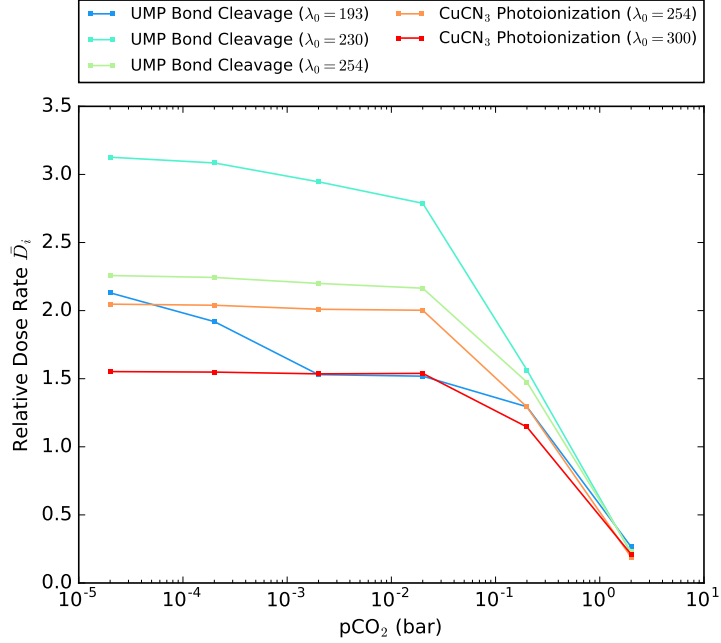


Fig. 12.— UV dose rates \bar{D}_i for clear-sky CO₂-H₂O atmospheres as a function of pCO₂ ($T_0 = 250\text{K}$, SZA=0, A corresponding to desert).

However, the sky was not necessarily clear during this epoch. In fact, formation of H₂O and CO₂ clouds are expected based on GCM studies (Wordsworth et al. 2013). Thick (though patchy) CO₂ cloud decks in particular are expected for thick CO₂ atmospheres. Figure 13 presents the dose rates \bar{D}_i as a function of CO₂ cloud optical depth for pCO₂=0.02 bar, SZA=0, and A corresponding to desert. As we might expect from Figure 5, the dose rate drops off only modestly with τ_{cloud} . $\tau_{cloud} \gtrsim 1000$ is required to suppress dose rates by more than an order of magnitude. For $r_{eff} = 10\mu\text{m}$, this corresponds to $20\times$ the maximum cloud column calculated by Wordsworth et al. (2013). Overall, the impact of clouds on their own on UV-sensitive photochemistry is expected to be modest.

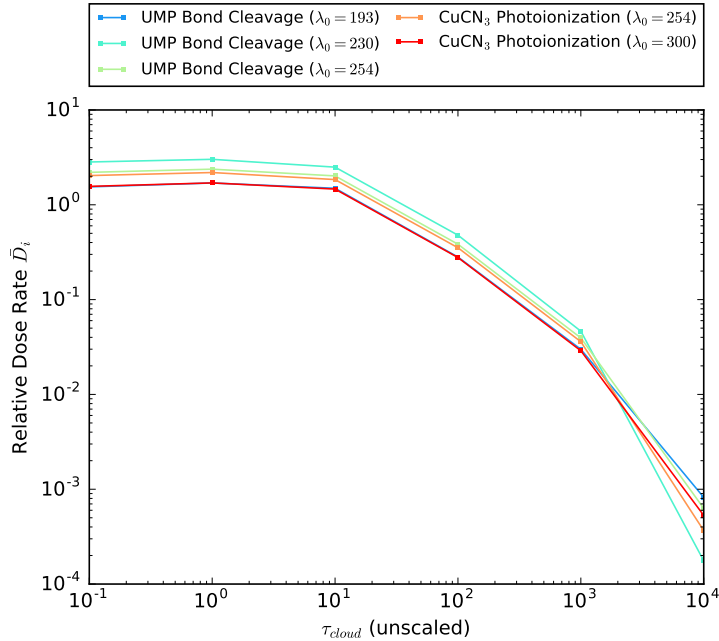


Fig. 13.— UV dose rates \bar{D}_i for $\text{CO}_2\text{-H}_2\text{O}$ atmospheres with a CO_2 cloud deck emplaced from 20-21 km altitude, as a function of cloud deck optical depth ($T_0 = 250\text{K}$, $\text{pCO}_2=0.02$ bar, $\text{SZA}=0$, A corresponding to desert).

If young Mars were indeed cold and dry, then one might expect it to have been dusty, as it is today. The modern Martian dust optical depth ranges from $\tau_d \sim 0.2 - 2$, with higher values achieved during dust storms (Smith et al. 2002; Lemmon et al. 2015). Higher dust loadings may have been possible when the atmosphere was thicker. Figure 14 presents the dose rates as a function of τ_d and pCO_2 , for $\text{SZA}=0$ and A corresponding to desert. Figure 15 presents the dose rates as a function of τ_d and CO_2 cloud optical depth, for $\text{SZA}=0$ and A corresponding to desert.

Unlike CO_2 and H_2O ice and gas, dust absorbs across the UV waveband. Further, this absorption can be dramatically increased in highly scattering atmospheres due to enhanced effective path length due to multiple scattering effects. Consequently, dust can dramatically suppress UV fluence and hence photochemistry, especially for thick and/or cloudy atmospheres. For $\tau_d \geq 10$, dose rates are suppressed by 2-8 orders of magnitude, depending on atmospheric pressure and cloud thickness. Dust of thickness $\tau_d = 1$ provides minimal suppression for $\text{pCO}_2 \leq 0.2$ bar or $\tau_{cloud} < 100$, but for $\text{pCO}_2 \geq 2$ bar or $\tau_{cloud} \geq 1000$, can suppress dose rates by orders of magnitude. Dust of thickness $\tau_d \leq 0.1$ does not significantly alter dose rates across the explored parameter space. Overall, dust can significantly alter

dose rates if it is present at high levels (greater than that seen for modern Martian dust storms) or if it is present at levels comparable to the modern average, but embedded in a thick atmosphere or underlying thick clouds.

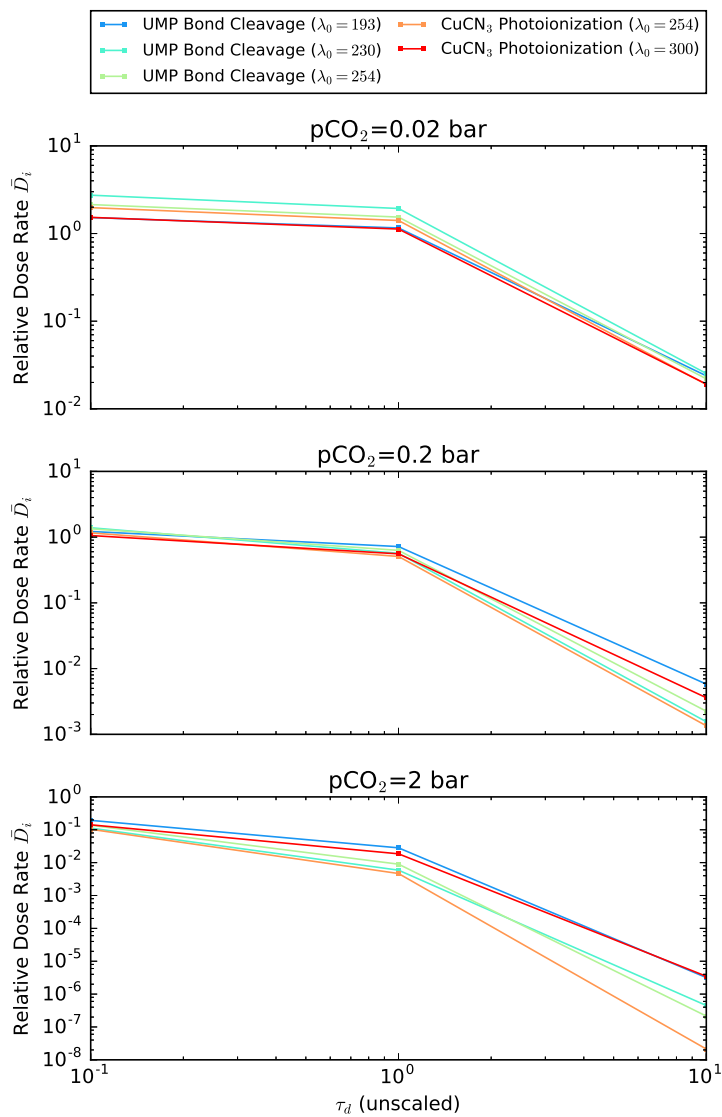


Fig. 14.— UV dose rates \bar{D}_i for dusty CO₂-H₂O atmospheres as a function of $p\text{CO}_2$ and τ_d ($T_0 = 250\text{K}$, $\text{SZA}=0$, A corresponding to desert).

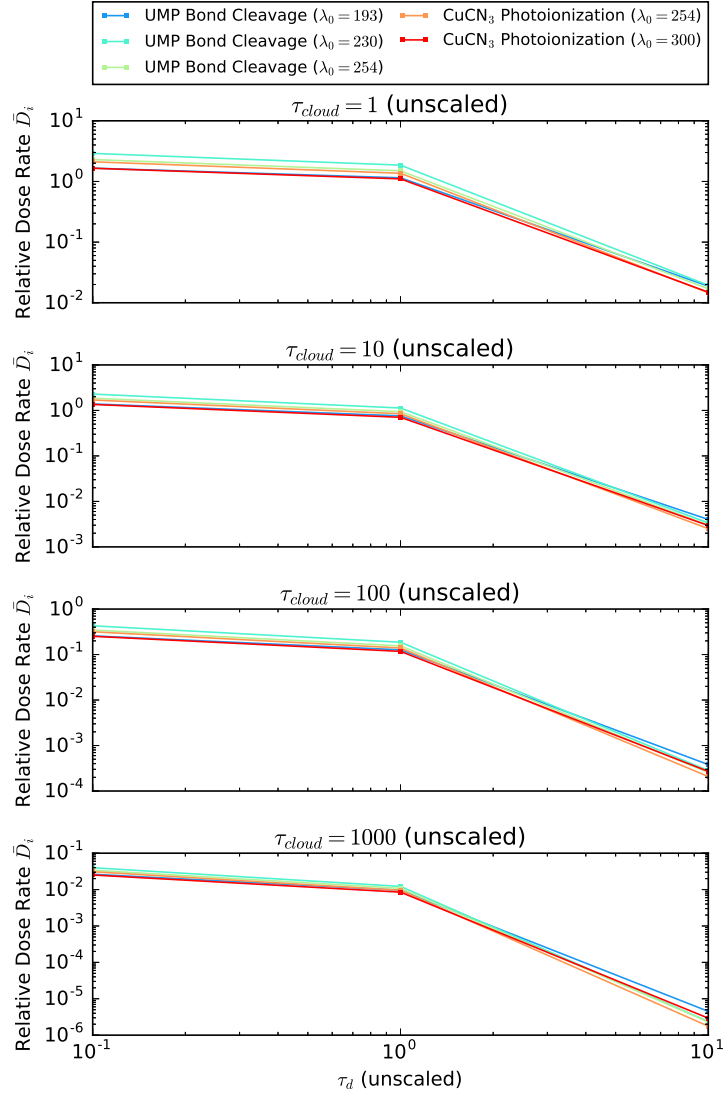


Fig. 15.— UV dose rates \bar{D}_i for dusty CO₂-H₂O atmospheres with a CO₂ cloud deck emplaced, as a function of τ_d and τ_{cloud} ($T_0 = 250\text{K}$, $p\text{CO}_2=0.02$, $\text{SZA}=0$, A corresponding to desert).

We considered the hypothesis that attenuation due to dust might differentially affect the stressor and eustressor pathways. That is, we considered the possibility that the eustressor reaction rates might fall off faster (or slower) than the stressor reaction rates with attenuation due to dust. Since the stressor pathway measures destruction of RNA monomers and the eustressor pathway measures a process important to the synthesis of key RNA precursors,

this means that environments that favor the eustressor pathway over the stressor pathway are a more favorable venue for abiogenesis than the reverse, in the RNA world hypothesis. This argument assumes that these particular stressor and eustressor processes were important in the prebiotic world. They might not have been. However, we expect other photochemical stressor and eustressor processes to behave in generally similar ways to these processes. For example, we generally expect the quantum yield of prebiotic molecular destruction to decrease with increasing wavelength because of decreased photon energy compared to bond strength. Similarly, regardless of the solvated electron source (e.g. HS^- as opposed to tricyanocuprate), we expect the quantum yield to go approximately as a step function in wavelength. We therefore suggest that results derived from these pathways may generalize to other processes, though a detailed comparison is required to rule on this hypothesis.

To assess the hypothesis that a dusty Mars might be less (or more) clement for abiogenesis than a non-dusty Mars as measured by our stressor (UMP-X) and eustressor (CuCN3-Y) pathways, we calculated $\overline{D}_{UMP-X}/\overline{D}_{CuCN3-Y}$. We calculated this quantity for $\text{pCO}_2 = 2$ bar (no clouds) and $\tau_{cloud} = 1000$ ($\text{pCO}_2=0.02$ bar) for $\tau_d = 0.1 - 10$. If these ratios rise with τ_d , it means that the stressor pathway is relatively favored by dusty atmospheres; if they fall, it means that the stressor pathway is relatively disfavored by dusty atmospheres.

Figure 16 presents these calculations. Dust attenuation on its own is relatively flat at CO_2 -scattering wavelengths, as is cloud attenuation. Consequently dusty/cloudy atmospheres tend to reduce UV fluence in a spectrally flat manner, and favor neither the stressor nor the eustressor pathway. On the other hand, in a thick CO_2 atmosphere, the scattering optical depth, and hence amplification of dust absorption, increases as wavelength decreases. Consequently, the dose rate ratio does change with increasing τ_d . However, the direction of the change is sensitive to the value of λ_0 , the ionization threshold for the tricyanocuprate ionization process, and the magnitude is further sensitive to the value of λ_0 for the UMP cleavage process. We consequently conclude it is possible that thick, dusty atmospheres might be more or less clement for abiogenesis than non-dusty atmospheres, but determining which requires wavelength-dependent measurements of the QYs of these chemical processes in the laboratory.

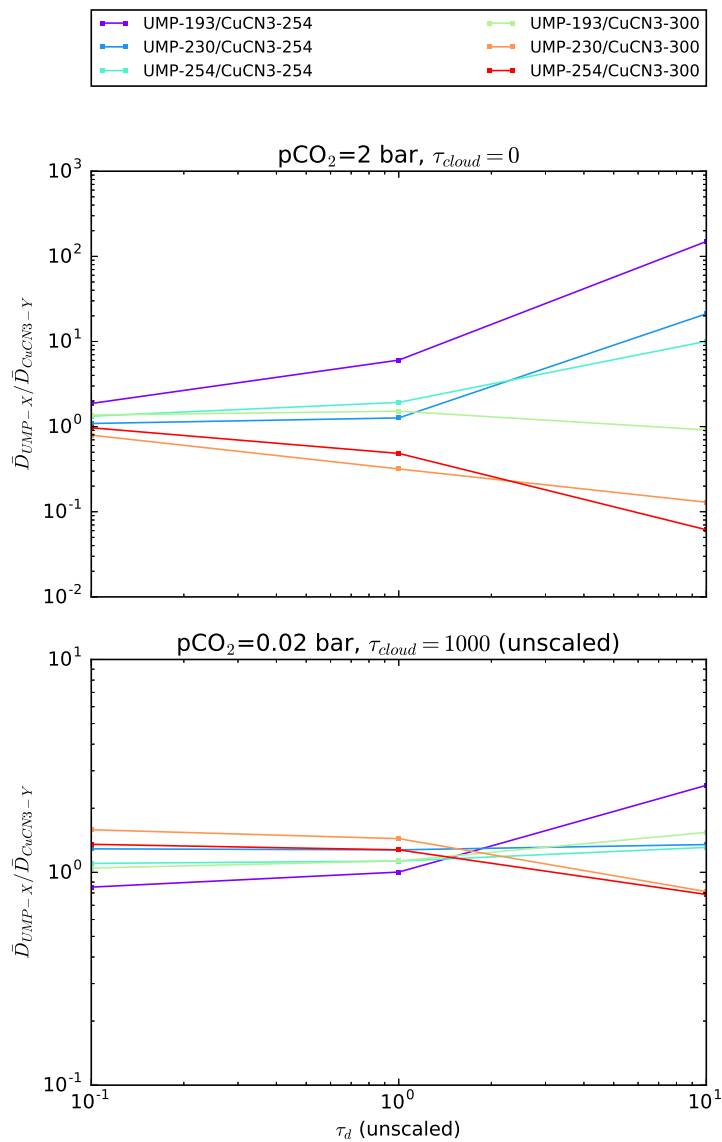


Fig. 16.— Ratio of stressor dose rates UMP-X divided by eustressor dose rates UMP-Y for dusty CO₂-H₂O atmospheres, as a function of τ_d ($T_0 = 250\text{K}$, SZA=0, A corresponding to desert). The atmospheres are highly scattering, either because of high pCO₂ or thick CO₂ clouds. Lower ratios imply a more favorable environment for abiogenesis as measured by these two photoprocesses.

5.2. Highly Reducing Atmospheres

Recent work suggests that if the reduced gases H_2 and/or CH_4 were present at elevated levels in a thick (~ 1 bar) atmosphere, collision-induced absorption (CIA) due to the interaction of these gases with CO_2 might provide enough greenhouse warming to elevate mean Noachian temperatures above freezing (Ramirez et al. 2014; Wordsworth et al. 2017). Ramirez et al. (2014) found that global mean surface temperatures exceeded 273K for $P_0 \geq 3$ bar and $[\text{H}_2] \geq 0.05$, with higher concentrations of H_2 required for lower P_0 . More recently, Wordsworth et al. (2017) used new ab initio calculations of $\text{H}_2\text{-CO}_2$ and $\text{CH}_4\text{-CO}_2$ CIA to show earlier estimates of the CIA were underestimated, and that 2-10% levels of CH_4 or H_2 in a > 1.25 bar atmosphere could elevate planetary mean temperatures over freezing. While it is unclear if such high reducing conditions can be sustained in the steady state, this scenario remains an intriguing avenue to a Noachian Mars with conditions at least transiently globally clement for liquid water and prebiotic chemistry (Batalha et al. 2015; Wordsworth et al. 2017).

H_2 is spectrally inert at UV wavelengths compared to CO_2 . Based on the constraints on H_2 absorption we found (Backx et al. 1976; Victor and Dalgarno 1969), the contribution of H_2 to atmospheric absorption and scattering are negligible for H_2 mixing ratios of 0 – 0.1. Similarly, CH_4 does not absorb at wavelengths longer than 165 nm (Au et al. 1993; Chen and Wu 2004). Hence, its absorption is highly degenerate with CO_2 , and its presence at the levels suggested in Wordsworth et al. (2017) does not impact the UV surface environment. Photochemically-generated hydrocarbon hazes require CH_4/CO_2 ratios of > 0.1 , and are consequently expected to be thin or nonexistent in this scenario (DeWitt et al. 2009). Consequently, the UV surface environment in an H_2 or CH_4 -rich atmosphere should be similar to the $p\text{CO}_2=2$ bar case discussed in Section 5.1.

5.3. Highly-Volcanic Mars ($\text{CO}_2\text{-H}_2\text{O-SO}_2/\text{H}_2\text{S}$ Atmosphere)

We have so far considered atmospheres with CO_2 and H_2O as their dominant photoactive gaseous species. However, other gases have been proposed as significant constituents of the Martian atmosphere. In particular, Halevy et al. (2007) suggest that the lack of massive carbonate deposits on Mars could have been explained if, during epochs of high volcanism on young Mars, SO_2 built up to the $\sim 1 - 100$ ppm level. At such levels, Halevy et al. (2007) find that SO_2 would supplant CO_2 as the agent regulating global chemistry and climate, inhibiting massive carbonate precipitation in the process. Halevy and Head (2014) further argue that enhanced radiative forcing from high SO_2 levels could transiently raise mean surface temperatures at the subsolar point (assuming no horizontal heat transport)

above the freezing point of water, explaining the observed fluvial features. Halevy and Head (2014) calculate that SO_2 mixing ratios $\gtrsim 10$ ppm (1 bar atmosphere) could have been possible during, e.g., the emplacement of the Martian volcanic plains. While the impact of SO_2 on Martian carbonates and climate remains debated (e.g., Niles et al. 2013, Kerber et al. 2015), it remains plausible that Noachian Mars may have been characterized by at least transiently high SO_2 levels due to higher volcanic outgassing rates.

We consequently sought to explore the impact of elevated levels of SO_2 on the UV surface environment and hence prebiotic chemistry. Figure 17 presents the dose rates calculated for a clear-sky atmosphere with varying $p\text{SO}_2$ and $p\text{CO}_2$. Figure 18 presents the dose rates calculated for an atmosphere with $p\text{CO}_2=0.02$ bar (optically thin at scattering wavelengths), but varying levels of CO_2 clouds. In both cases, $\text{SZA}=0$ and A corresponds to desert.

SO_2 is a far broader, stronger UV absorber than either CO_2 or H_2O , and consequently its presence can exert a dramatic impact on UV surface radiance and photochemistry rates. As with dust, multiple scattering from other atmospheric constituents can amplify SO_2 absorption. For $p\text{CO}_2 \leq 0.2$ bar, $p\text{SO}_2 \geq 2 \times 10^{-6}$ bar is required to suppress dose rates to $\overline{D}_i < 0.1$, whereas for $p\text{CO}_2 \geq 2$ bar, $p\text{SO}_2 \geq 2 \times 10^{-7}$ bar is sufficient. Similarly, for $\tau_{cloud} \leq 10$, $p\text{SO}_2 \geq 2 \times 10^{-6}$ bar is required to suppress dose rates to $\overline{D}_i < 0.1$, whereas for $\tau_{cloud} \geq 100$, $p\text{SO}_2 \geq 2 \times 10^{-7}$ bar is sufficient. For $p\text{SO}_2 \geq 2 \times 10^{-5}$ bar, UV-sensitive prebiotic photochemistry is strongly quenched.

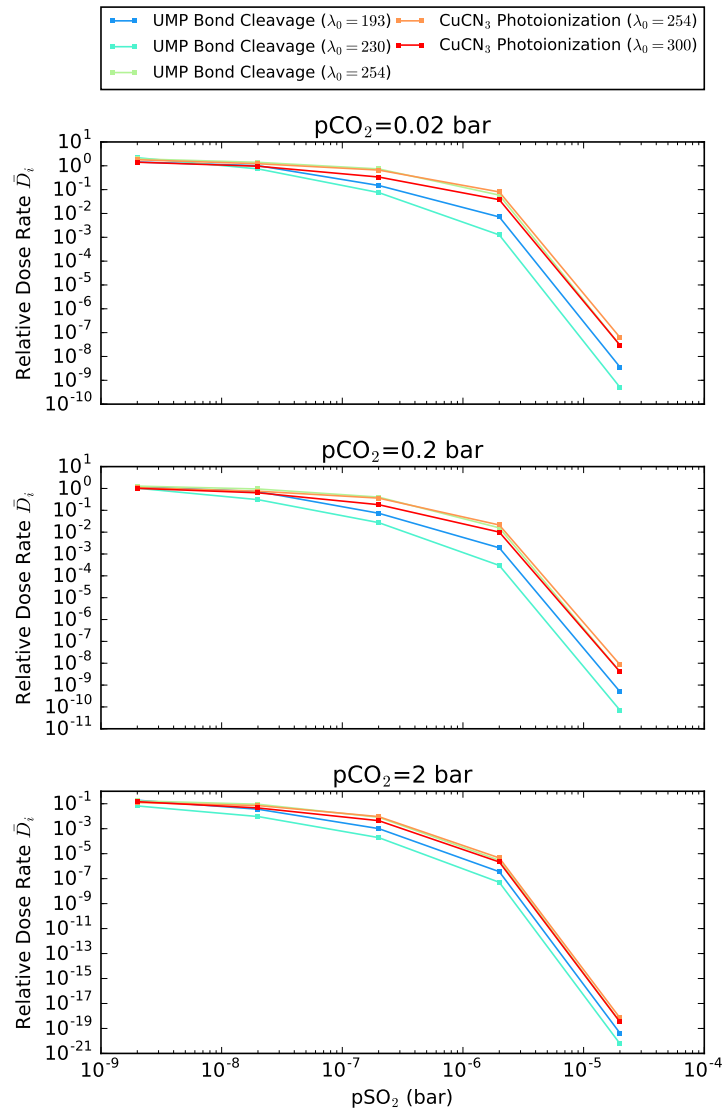


Fig. 17.— UV dose rates \bar{D}_i for $\text{CO}_2\text{-H}_2\text{O-SO}_2$ atmospheres as a function of $p\text{CO}_2$ and $p\text{SO}_2$ ($T_0 = 250\text{K}$, $\text{SZA}=0$, A corresponding to desert).

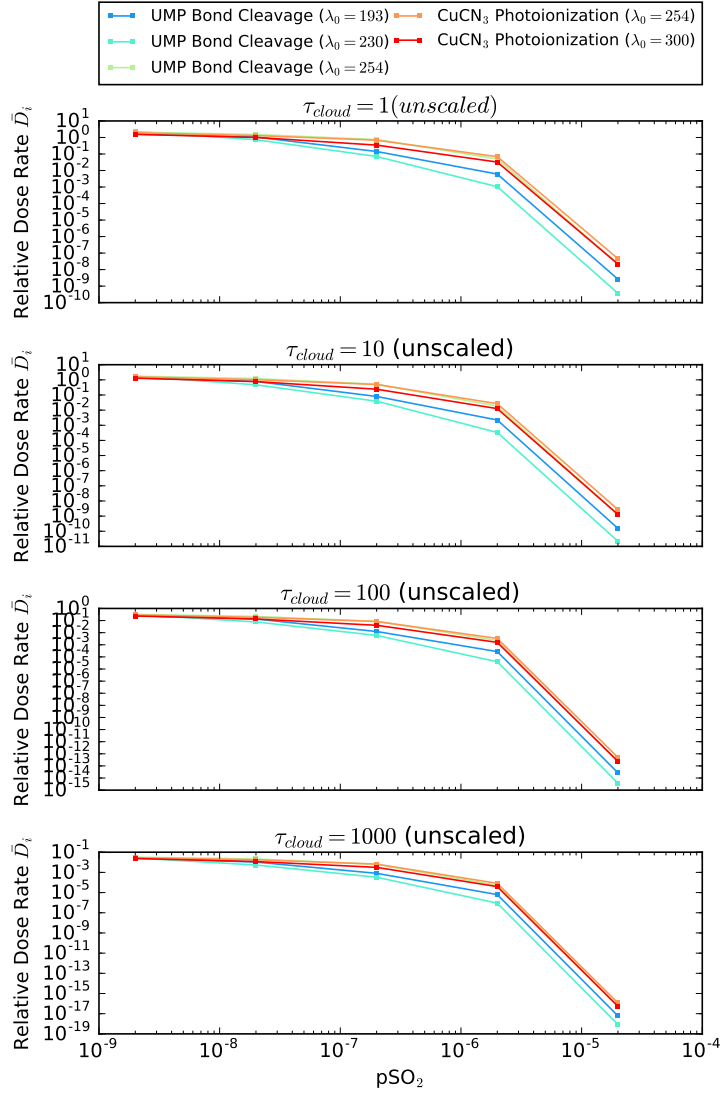


Fig. 18.— UV dose rates \bar{D}_i for $\text{CO}_2\text{-H}_2\text{O-SO}_2$ atmospheres with a CO_2 cloud deck emplaced, as a function of $p\text{SO}_2$ and τ_{cloud} ($T_0 = 250\text{K}$, $p\text{CO}_2=0.02\text{SZA}=0$, A corresponding to desert).

As with dust, we considered the hypothesis that attenuation from SO_2 might have a differential impact on the eustressor and stressor pathways. We calculated $\bar{D}_{UMP-X}/\bar{D}_{CuCN3-Y}$ for $p\text{CO}_2 = 2$ bar (no clouds) and $\tau_{cloud} = 1000$ ($p\text{CO}_2=0.02$ bar) for a broad range of $p\text{SO}_2$. This calculation is presented in Figure 19. We note that regardless of assumption on λ_0 , as $p\text{SO}_2$ increases from $2 \times 10^{-7} - 2 \times 10^{-5}$ bar, the eustressor pathway is favored over the stressor pathways, by as much as 2 orders of magnitude (dependent on λ_0). We conclude that it

seems plausible that high-SO₂ planetary atmospheres have a UV throughput more clement for abiogenesis compared to low-SO₂ atmospheres under the assumption that the stressor and eustressor pathways we have identified were important. However, better measurements of the spectral QY of these photoprocesses is required to confirm and quantify the magnitude of this effect.

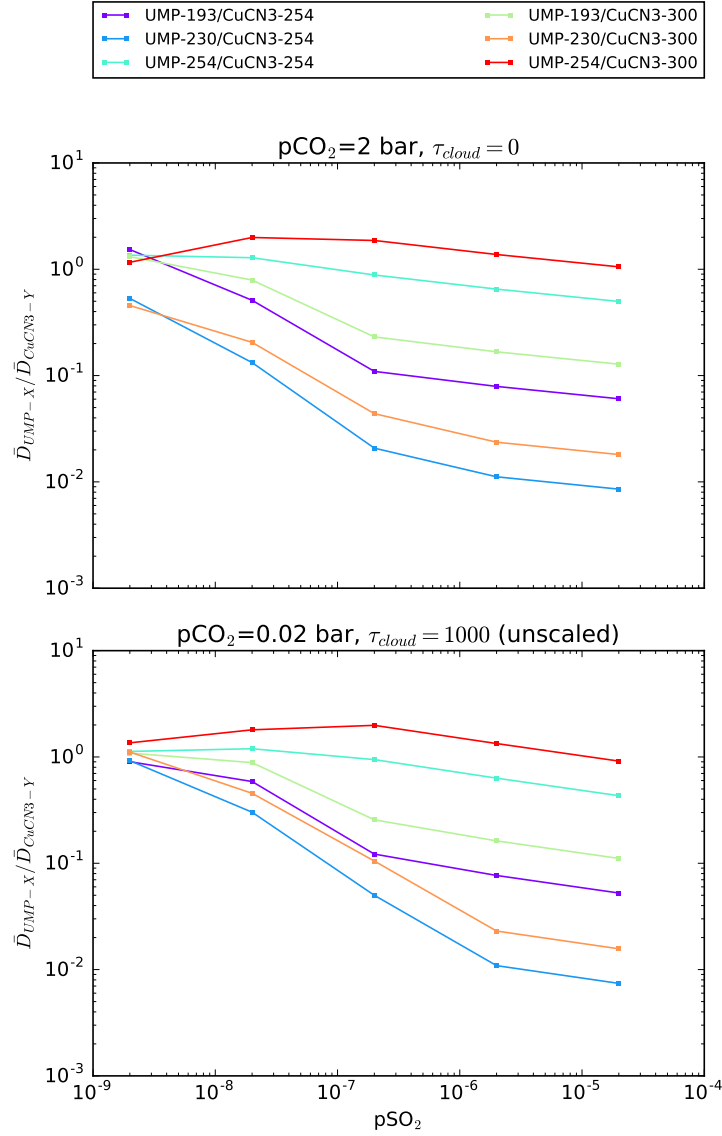


Fig. 19.— Ratio of stressor dose rates UMP-X divided by eustressor dose rates UMP-Y for CO₂-H₂O-SO₂ atmospheres, as a function of pSO₂ ($T_0 = 250K$, $SZA=0$, A corresponding to desert). The atmospheres are highly scattering, either because of high pCO₂ or thick CO₂ clouds. Lower ratios imply a more favorable environment for abiogenesis as measured by these two photoprocesses.

While Halevy and Head (2014) focused on the abundance of SO₂ in the Martian atmosphere, H₂S is emitted in equal proportion by the more reduced Martian mantle Halevy et al. (2007). Hu et al. (2013) model the atmospheric composition as a function of sulfur

emission rate for a 1-bar CO_2 atmosphere assuming equipartition of the outgassed sulfur between SO_2 and H_2S , irradiated by a G2V star at a distance of 1.3 AU. They find H_2S concentrations to be even higher than SO_2 concentrations, by over an order of magnitude at high S emission rates. H_2S is also a stronger, broader UV absorber than CO_2 or H_2O . Consequently, we sought to explore the impact of elevated levels of H_2S on the UV surface environment and prebiotic photochemistry.

Figure 20 presents the dose rates calculated for a clear-sky atmosphere with varying pH_2S and pCO_2 . Figure 21 presents the dose rates calculated for an atmosphere with $\text{pCO}_2=0.02$ bar (optically thin at scattering wavelengths), but varying levels of CO_2 clouds. In both cases, $\text{SZA}=0$ and A corresponding to desert. As with SO_2 and dust, highly scattering atmospheres can amplify H_2S absorption. For $\text{pCO}_2 \leq 0.2$ bar, $\overline{D}_i < 0.1$ for $\text{pH}_2\text{S} \geq 2 \times 10^{-5}$ bar, but for $\text{pCO}_2 \geq 2$ bar, $\overline{D}_i < 0.1$ for $\text{pH}_2\text{S} \geq 2 \times 10^{-6}$ bar. Similarly, for $\tau_{cloud} \leq 10$, $\overline{D}_i < 0.1$ for $\text{pH}_2\text{S} \geq 2 \times 10^{-5}$ bar, but for $\tau_{cloud} \geq 100$, $\overline{D}_i \lesssim 0.1$ for $\text{pH}_2\text{S} \geq 2 \times 10^{-6}$ bar. For $\text{pH}_2\text{S} \geq 2 \times 10^{-4}$ bar, surface photochemistry is strongly quenched regardless of atmospheric state.

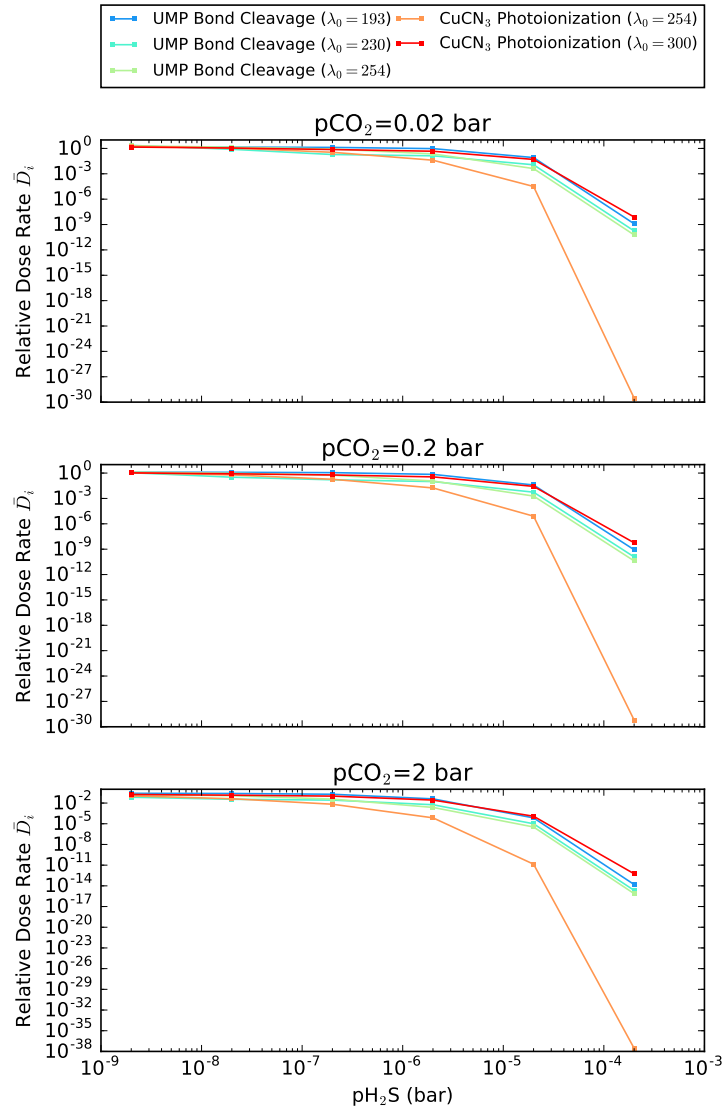


Fig. 20.— UV dose rates \bar{D}_i for $\text{CO}_2\text{-H}_2\text{O-H}_2\text{S}$ atmospheres as a function of pCO_2 and pH_2S ($T_0 = 250\text{K}$, $\text{SZA}=0$, A corresponding to desert).

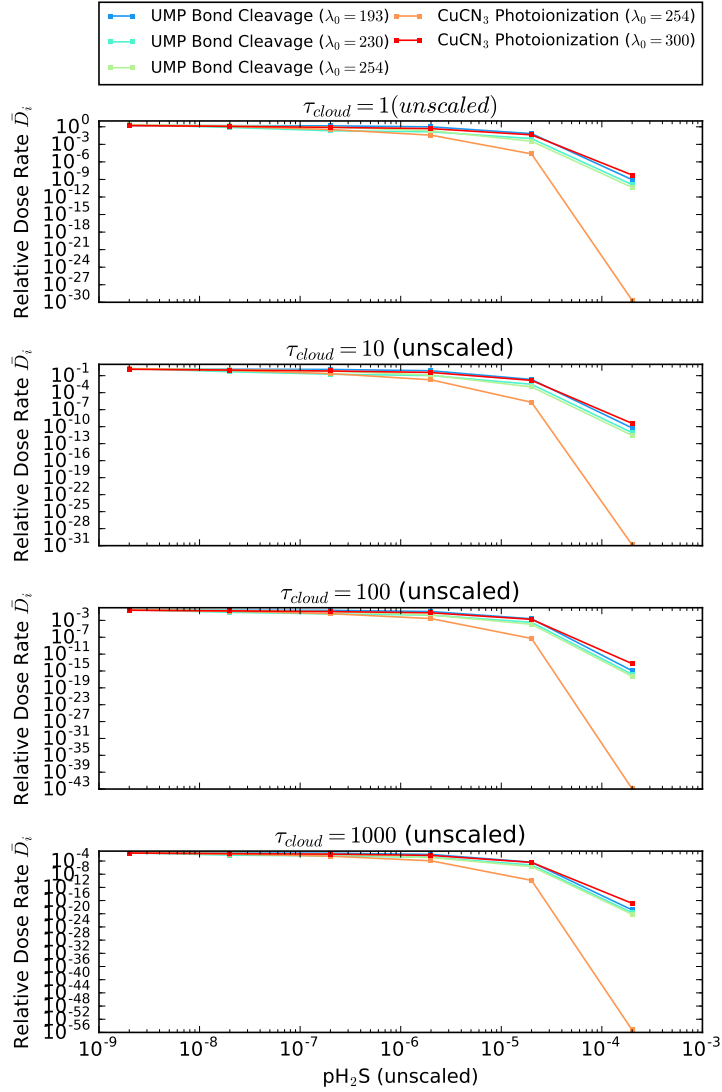


Fig. 21.— UV dose rates \bar{D}_i for $\text{CO}_2\text{-H}_2\text{O-H}_2\text{S}$ atmospheres with a CO_2 cloud deck emplaced, as a function of pH_2S and τ_{cloud} ($T_0 = 250\text{K}$, $\text{pCO}_2=0.02$ bar, $\text{SZA}=0$, A corresponding to desert).

We again considered the hypothesis that H_2S attenuation might have a differential impact on the stressor and eustressor dose rates. We calculated $\bar{D}_{UMP-X}/\bar{D}_{CuCN3-Y}$ for $\text{pCO}_2 = 2$ bar (no clouds) and $\tau_{cloud} = 1000$ ($\text{pCO}_2=0.02$ bar) for a broad range of pH_2S . This calculation is presented in Figure 22. As in the case of dust in a dense CO_2 atmosphere, the ratios diverge from 1, but in opposite directions depending on the value assumed for λ_0 for

photoionization of tricyanocuprate. We conclude that attenuation from H₂S may well have a differential impact on the stressor and eustressor dose rates, but that assessing which it favors requires better constraints on the QYs of the photoprocesses, especially the photoionization of tricyanocuprate.

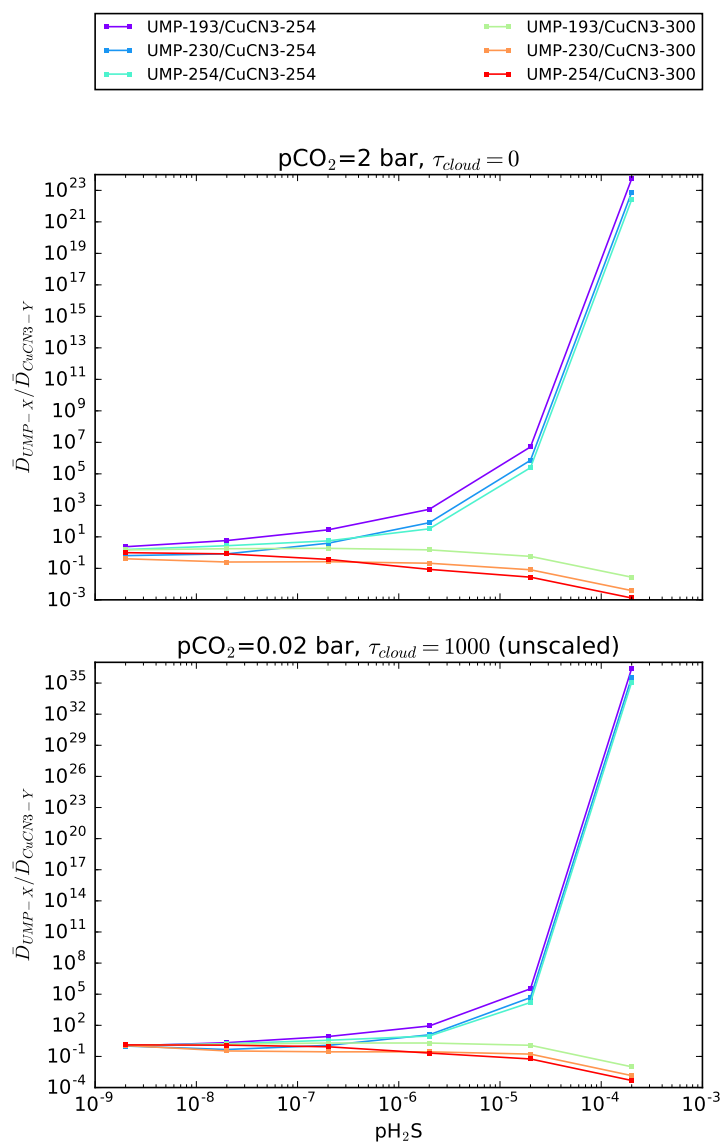


Fig. 22.— Ratio of stressor dose rates UMP-X divided by eustressor dose rates UMP-Y for CO₂-H₂O-H₂S atmospheres, as a function of pH₂S ($T_0 = 250\text{K}$, SZA=0, A corresponding to desert). The atmospheres are highly scattering, either because of high pCO₂ or thick CO₂ clouds. Lower ratios imply a more favorable environment for abiogenesis as measured by these two photoprocesses.

6. Conclusion

We have used a two-stream multi-layer radiative transfer model to estimate the UV surface environment on the surface of 3.9 Ga Mars as a function of atmospheric composition, and explored the implications for prebiotic chemistry. Prebiotic photoreaction rates are within an order of magnitude of the terrestrial values for normative clear-sky CO₂-H₂O atmospheres, in agreement with past work (e.g., Cockell 2000) suggesting early Martian and terrestrial atmospheres featured comparable UV environments. In agreement with prior work, we find shortwave radiation to be effectively attenuated by CO₂ absorption, with fluence \lesssim 185 nm removed for pCO₂ \geq 2×10^{-5} bar and fluence $<$ 204 nm removed for pCO₂ \geq 0.2 bar. Fluence drops off more slowly in the $>$ 204 nm regime, where neither CO₂ nor H₂O absorb. This is a consequence of random walk statistics in highly scattering regimes, and stands in contrast to prior studies (Rontó et al. 2003; Cnossen et al. 2007) which did not account for multiple scattering. The impact of CO₂ and H₂O clouds on their own is similarly muted because they too are pure scatterers in the $>$ 204 nm regime; $\tau_{cloud} \geq 100$ is required to significantly affect surficial reaction rates, comparable to but in excess of the highest patchy cloud optical depths predicted by some 3D GCM studies (e.g., Wordsworth et al. 2013).

While dense atmospheres and cloud decks only modestly reduce surface fluence on their own, in concert with other absorbers (dust, SO₂, H₂S) they can have a dramatic effect on surface fluence and reaction rates, though amplification of the effects of these absorbers. Dust levels of $\tau_d = 1$, only a factor of a few higher than that sustained in the modern atmosphere, could suppress prebiotic reaction rates by orders of magnitude for pCO₂ \geq 2bar or $\tau_{cloud} \geq 1000$, and dust levels of $\tau_d = 10$ would sharply reduce reaction rates independent of the atmospheric state. Similarly, pSO₂ $\geq 10^{-7}$ bar or pH₂S $\geq 2 \times 10^{-6}$ bars are required to significantly reduce reaction rates for pCO₂ \geq 2bar or $\tau_{cloud} \geq 100$, but for less scattering atmospheres, pSO₂ $\geq 10^{-6}$ bar or pH₂S $\geq 2 \times 10^{-5}$ bar is required. pSO₂ $\geq 10^{-5}$ bars or pH₂S $\geq 2 \times 10^{-4}$ bars quenches UV-sensitive photochemistry by many orders of magnitude regardless of other atmospheric conditions.

The absorbers described above have spectrally variable absorption, and prebiotic photochemistry is wavelength-dependent, leading us to speculate whether high abundances of these absorbers, despite suppressing UV-sensitive chemistry generally, might not favor or disfavor eustressor photoprocesses conducive to the origin of life compared to stressor processes that impede life's formation. We compare the relative impact of absorption from dust, SO₂, and H₂S attenuation on two such stressor (cleavage of the N-glycosidic bond of UMP) and eustressor photoprocesses (production of aquated electrons from CuCN₃²⁻). We find that it is possible for high levels of these absorbers to disproportionately favor one or the other

of these photoprocesses. In particular, high SO₂ levels may create an especially favorable environment for abiogenesis, under the assumption that these photoprocesses were important to abiogenesis (so long as enough fluence reaches the ground to power these reactions). However, the magnitude and direction of this effect is sensitive to assumptions about the QY of these processes. Better characterization of the spectral quantum yields of these processes are required to rule definitively on this question.

7. Acknowledgements

We thank C. Magnani and S. Rugheimer for sharing their data with us, and for many insightful conversations. We thank J. Sutherland and J. Szostak for sharing their insights into prebiotic chemistry. We thank two anonymous referees, whose comments improved this manuscript.

This research has made use of NASA’s Astrophysics Data System Bibliographic Services, and the MPI-Mainz UV-VIS Spectral Atlas of Gaseous Molecules.

S. R. and D. D. S. gratefully acknowledge support from the Simons Foundation, grant no. 290360.

8. Author Disclosure Statement

The authors declare no competing financial interests.

REFERENCES

- Adcock, C. T., E. M. Hausrath, and P. M. Forster (2013). Readily available phosphate from minerals in early aqueous environments on Mars. *Nature Geoscience* 6(10), 824–827.
- Au, J. W., G. Cooper, G. R. Burton, T. N. Olney, and C. Brion (1993). The valence shell photoabsorption of the linear alkanes, C_nH_{2n+2} ($n=1-8$): absolute oscillator strengths (7–220 eV). *Chemical physics* 173(2), 209–239.
- Backx, C., G. R. Wight, and M. J. Van der Wiel (1976, February). Oscillator strengths (10–70 eV) for absorption, ionization and dissociation in H_2 , HD and D_2 , obtained by an electron-ion coincidence method. *Journal of Physics B Atomic Molecular Physics* 9, 315–331.
- Batalha, N., S. D. Domagal-Goldman, R. Ramirez, and J. F. Kasting (2015, September). Testing the early Mars H_2 - CO_2 greenhouse hypothesis with a 1-D photochemical model. *Icarus* 258, 337–349.
- Benner, S. A. (2013). Planets, Minerals and Life’s Origin. *Mineralogical Magazine* 77(5), 686.
- Benner, S. A., H.-j. K. Foundation, and A. Fl (2015). The Case for a Martian Origin for Earth Life. In R. B. Hoover, G. V. Levin, A. Y. Rozanov, and N. C. Wickramasinghe (Eds.), *Instruments, Methods and Missions for Astrobiology XVII*, Volume 9606, pp. 1–16.
- Benner, S. A., H.-J. Kim, M.-J. Kim, and A. Ricardo (2010). Planetary organic chemistry and the origins of biomolecules. *Cold Spring Harbor perspectives in biology* 2(7), a003467.
- Bohren, C. F. (1987, June). Multiple scattering of light and some of its observable consequences. *American Journal of Physics* 55, 524–533.
- Bristow, T. F., D. L. Bish, D. T. Vaniman, R. V. Morris, D. F. Blake, J. P. Grotzinger, E. B. Rampe, J. A. Crisp, C. N. Achilles, D. W. Ming, B. L. Ehlmann, P. L. King, J. C. Bridges, J. L. Eigenbrode, D. Y. Sumner, S. J. Chipera, J. M. Moorokian, A. H. Treiman, S. M. Morrison, R. T. Downs, J. D. Farmer, D. Des Marais, P. Sarrazin, M. M. Floyd, M. A. Mischna, and A. C. McAdam (2015). The origin and implications of clay minerals from Yellowknife Bay, Gale crater, Mars. *American Mineralogist* 100(4), 824–836.

- Chen, F. and C. Wu (2004, May). Temperature-dependent photoabsorption cross sections in the VUV-UV region. I. Methane and ethane. *Journal of Quantitative Spectroscopy and Radiative Transfer* 85(2), 195–209.
- Claire, M. W., J. Sheets, M. Cohen, I. Ribas, V. S. Meadows, and D. C. Catling (2012, September). The Evolution of Solar Flux from 0.1 nm to 160 μm : Quantitative Estimates for Planetary Studies. *ApJ* 757, 95.
- Cnossen, I., J. Sanz-Forcada, F. Favata, O. Witasse, T. Zegers, and N. F. Arnold (2007, February). Habitat of early life: Solar X-ray and UV radiation at Earth’s surface 4-3.5 billion years ago. *Journal of Geophysical Research (Planets)* 112, 2008.
- Cockell, C. (2000). The ultraviolet history of the terrestrial planets: implications for biological evolution. *Planetary and Space Science* 48.
- Cockell, C. S. (1999). Carbon biochemistry and the ultraviolet radiation environments of F, G, and K main sequence stars. *Icarus* 141(2), 399–407.
- Cockell, C. S. (2002). Photobiological uncertainties in the archaean and post-archaean world. *International Journal of Astrobiology* 1(01), 31–38.
- Colaprete, A. and O. B. Toon (2003, April). Carbon dioxide clouds in an early dense Martian atmosphere. *Journal of Geophysical Research (Planets)* 108, 6–1.
- DeWitt, H. L., M. G. Trainer, A. A. Pavlov, C. A. Hasenkopf, A. C. Aiken, J. L. Jimenez, C. P. McKay, O. B. Toon, and M. A. Tolbert (2009, June). Reduction in Haze Formation Rate on Prebiotic Earth in the Presence of Hydrogen. *Astrobiology* 9, 447–453.
- Fanale, F. P., J. R. Salvail, W. B. Banerdt, and R. S. Saunders (1982, June). Mars - The regolith-atmosphere-cap system and climate change. *Icarus* 50, 381–407.
- Forget, F., F. Hourdin, R. Fournier, C. Hourdin, O. Talagrand, M. Collins, S. R. Lewis, P. L. Read, and J.-P. Huot (1999). Improved general circulation models of the martian atmosphere from the surface to above 80 km. *Journal of Geophysical Research: Planets* 104(E10), 24155–24175.
- Forget, F. and R. T. Pierrehumbert (1997). Warming early mars with carbon dioxide clouds that scatter infrared radiation. *Science* 278(5341), 1273–1276.
- Forget, F., R. Wordsworth, E. Millour, J.-B. Madeleine, L. Kerber, J. Leconte, E. Marcq, and R. M. Haberle (2013, January). 3D modelling of the early martian climate under a denser CO₂ atmosphere: Temperatures and CO₂ ice clouds. *Icarus* 222, 81–99.

- Gollihar, J., M. Levy, and A. D. Ellington (2014). Many paths to the origin of life. *Science* *343*(6168), 259–260.
- Grotzinger, J. P., S. Gupta, M. C. Malin, D. M. Rubin, J. Schieber, K. Siebach, D. Y. Sumner, K. M. Stack, a. R. Vasavada, R. E. Arvidson, F. Calef, L. Edgar, W. F. Fischer, J. a. Grant, J. Griffes, L. C. Kah, M. P. Lamb, K. W. Lewis, N. Mangold, M. E. Minitti, M. Palucis, M. Rice, R. M. E. Williams, R. a. Yingst, D. Blake, D. Blaney, P. Conrad, J. Crisp, W. E. Dietrich, G. Dromart, K. S. Edgett, R. C. Ewing, R. Gellert, J. a. Hurowitz, G. Kocurek, P. Mahaffy, M. J. McBride, S. M. McLennan, M. Mischna, D. Ming, R. Milliken, H. Newsom, D. Oehler, T. J. Parker, D. Vaniman, R. C. Wiens, and S. a. Wilson (2015). Deposition, exhumation, and paleoclimate of an ancient lake deposit, Gale crater, Mars. *Science (New York, N.Y.)* *350*(6257), aac7575.
- Gurzadyan, G. G. and H. Görner (1994). Damage to uracil-and adenine-containing bases, nucleosides, nucleotides and polynucleotides: Quantum yields on irradiation at 193 and 254 nm. *Photochemistry and photobiology* *60*(4), 323–332.
- Halevy, I. and J. W. Head, III (2014, December). Episodic warming of early Mars by punctuated volcanism. *Nature Geoscience* *7*, 865–868.
- Halevy, I., M. T. Zuber, and D. P. Schrag (2007, dec). A sulfur dioxide climate feedback on early Mars. *Science (New York, N.Y.)* *318*(5858), 1903–7.
- Hansen, G. B. (1997, September). The infrared absorption spectrum of carbon dioxide ice from 1.8 to 333 μm . *J. Geophys. Res.* *102*, 21569–21588.
- Hansen, G. B. (2005, November). Ultraviolet to near-infrared absorption spectrum of carbon dioxide ice from 0.174 to 1.8 μm . *Journal of Geophysical Research (Planets)* *110*, E11003.
- Hansen, J. E. and L. D. Travis (1974, October). Light scattering in planetary atmospheres. *Space Sci. Rev.* *16*, 527–610.
- Herd, C. D. K., L. E. Borg, J. H. Jones, and J. J. Papike (2002, June). Oxygen fugacity and geochemical variations in the martian basalts: implications for martian basalt petrogenesis and the oxidation state of the upper mantle of Mars. *Geochim. Cosmochim. Acta* *66*, 2025–2036.
- Hoekzema, N. M., M. Garcia-Comas, O. J. Stenzel, B. Grieger, W. J. Markiewicz, K. Gwinner, and H. U. Keller (2010, June). Optical depth and its scale-height in Valles Marineris from HRSC stereo images. *Earth and Planetary Science Letters* *294*, 534–540.

- Horváth, A., S. Papp, and Z. Décsy (1984). Formation of aquated electrons and the individual quantum yields for photoactive species in the Cu (I)KCNH₂O system. *Journal of photochemistry* 24(4), 331–339.
- Hu, R., S. Seager, and W. Bains (2012, December). Photochemistry in Terrestrial Exoplanet Atmospheres. I. Photochemistry Model and Benchmark Cases. *ApJ* 761, 166.
- Hu, R., S. Seager, and W. Bains (2013, May). Photochemistry in Terrestrial Exoplanet Atmospheres. II. H₂S and SO₂ Photochemistry in Anoxic Atmospheres. *ApJ* 769, 6.
- Joseph, J. H., W. J. Wiscombe, and J. A. Weinman (1976, December). The delta-Eddington approximation for radiative flux transfer. *Journal of Atmospheric Sciences* 33, 2452–2459.
- Kasting, J. F. (1991, November). CO₂ condensation and the climate of early Mars. *Icarus* 94, 1–13.
- Kerber, L., F. Forget, and R. Wordsworth (2015, November). Sulfur in the early martian atmosphere revisited: Experiments with a 3-D Global Climate Model. *Icarus* 261, 133–148.
- Kirschvink, J. L. and B. P. Weiss (2002). Mars, panspermia, and the origin of life: where did it all begin. *Palaeontologia electronica* 4(2), 8–15.
- Kylling, A., K. Stamnes, and S. Tsay (1995). A reliable and efficient two-stream algorithm for spherical radiative transfer: Documentation of accuracy in realistic layered media. *Journal of Atmospheric Chemistry* 21(2), 115–150.
- Lemmon, M. T., M. J. Wolff, J. F. Bell, III, M. D. Smith, B. A. Cantor, and P. H. Smith (2015, May). Dust aerosol, clouds, and the atmospheric optical depth record over 5 Mars years of the Mars Exploration Rover mission. *Icarus* 251, 96–111.
- Madronich, S. (1987). Photodissociation in the atmosphere: 1. actinic flux and the effects of ground reflections and clouds. *Journal of Geophysical Research: Atmospheres* 92(D8), 9740–9752.
- Magnani, C. J. (2015). Life’s first steps: Exploring the feasibility of prebiotic chemical reactions through ultraviolet dependence. A.B. Thesis, Harvard University.
- Maher, K. A. and D. J. Stevenson (1988, February). Impact frustration of the origin of life. *Nature* 331, 612–614.

- Mayer, B., A. Kylling, S. Madronich, and G. Seckmeyer (1998, December). Enhanced absorption of UV radiation due to multiple scattering in clouds: Experimental evidence and theoretical explanation. *J. Geophys. Res.* *103*, 31.
- Miller, T. M. (2009). Atomic and molecular polarizabilities. In D. R. Lide (Ed.), *CRC Handbook of Chemistry and Physics* (90 ed.). Boca Raton, FL: CRC Press.
- Mishra, M. K., P. Chauhan, R. Singh, S. M. Moorthi, and S. S. Sarkar (2016, February). Estimation of dust variability and scale height of atmospheric optical depth (AOD) in the Valles Marineris on Mars by Indian Mars Orbiter Mission (MOM) data. *Icarus* *265*, 84–94.
- Mulkidjanian, A. Y., D. A. Cherepanov, and M. Y. Galperin (2003). Survival of the fittest before the beginning of life: selection of the first oligonucleotide-like polymers by UV light. *BMC Evolutionary Biology* *3*, 12.
- Niles, P. B., D. C. Catling, G. Berger, E. Chassefière, B. L. Ehlmann, J. R. Michalski, R. Morris, S. W. Ruff, and B. Sutter (2013). Geochemistry of carbonates on mars: implications for climate history and nature of aqueous environments. *Space Science Reviews* *174*(1-4), 301–328.
- Pang, K. and J. M. Ajello (1977, January). Complex refractive index of Martian dust - Wavelength dependence and composition. *Icarus* *30*, 63–74.
- Parkinson, W. H., J. Rufus, and K. Yoshino (2003, May). Absolute absorption cross section measurements of CO₂ in the wavelength region 163-200 nm and the temperature dependence. *Chemical Physics* *290*, 251–256.
- Patel, B. H., C. Percivalle, D. J. Ritson, C. D. Duffy, and J. D. Sutherland (2015). Common origins of RNA, protein and lipid precursors in a cyanosulfidic protometabolism. *Nature Chemistry* (March), 1–7.
- Pierrehumbert, R. T. (2010). *Principles of planetary climate*. Cambridge University Press.
- Powner, M. W., B. Gerland, and J. D. Sutherland (2009, may). Synthesis of activated pyrimidine ribonucleotides in prebiotically plausible conditions. *Nature* *459*(7244), 239–42.
- Ramirez, R. M., R. Kopparapu, M. E. Zugger, T. D. Robinson, R. Freedman, and J. F. Kasting (2014). Warming early mars with co₂ and h₂. *Nature Geoscience* *7*(1), 59–63.

- Ranjan, S. and D. D. Sasselov (2016, January). Influence of the UV Environment on the Synthesis of Prebiotic Molecules. *Astrobiology* 16, 68–88.
- Ranjan, S. and D. D. Sasselov (2017, March). Constraints on the Early Terrestrial Surface UV Environment Relevant to Prebiotic Chemistry. *Astrobiology* 17, 169–204.
- Rapf, R. J. and V. Vaida (2016). Sunlight as an energetic driver in the synthesis of molecules necessary for life. *Phys. Chem. Chem. Phys.* 18, 20067–20084.
- Ritson, D. and J. D. Sutherland (2012, November). Prebiotic synthesis of simple sugars by photoredox systems chemistry. *Nature chemistry* 4(11), 895–9.
- Robinson, T. D. and D. C. Catling (2014, January). Common 0.1bar tropopause in thick atmospheres set by pressure-dependent infrared transparency. *Nature Geoscience* 7, 12–15.
- Rontó, G., A. Bérces, H. Lammer, C. S. Cockell, G. J. Molina-Cuberos, M. R. Patel, F. Selsis, and A. Be (2003). Solar UV irradiation conditions on the surface of Mars. *Photochemistry and photobiology* 77(1), 34–40.
- Rosenberg, R., M. Abu Haija, and P. Ryan (2008, October). Chiral-Selective Chemistry Induced by Spin-Polarized Secondary Electrons from a Magnetic Substrate. *Physical Review Letters* 101(17), 178301.
- Rugheimer, S., A. Segura, L. Kaltenegger, and D. Sasselov (2015, June). UV Surface Environment of Earth-like Planets Orbiting FGKM Stars through Geological Evolution. *ApJ* 806, 137.
- Sagan, C. (1973, April). Ultraviolet selection pressure on the earliest organisms. *Journal of theoretical biology* 39(1), 195–200.
- Sarker, P. K., J.-i. Takahashi, Y. Obayashi, T. Kaneko, and K. Kobayashi (2013, June). Photo-alteration of hydantoins against UV light and its relevance to prebiotic chemistry. *Advances in Space Research* 51(12), 2235–2240.
- Segura, A., V. S. Meadows, J. F. Kasting, D. Crisp, and M. Cohen (2007, September). Abiotic formation of O₂ and O₃ in high-CO₂ terrestrial atmospheres. *A&A* 472, 665–679.
- Sinsheimer, R. L. and R. Hastings (1949). A reversible photochemical alteration of uracil and uridine. *Science* 110(2864), 525–526.
- Sleep, N. H., K. J. Zahnle, J. F. Kasting, and H. J. Morowitz (1989, November). Annihilation of ecosystems by large asteroid impacts on the early earth. *Nature* 342, 139–142.

- Smith, M. D., B. J. Conrath, J. C. Pearl, and P. R. Christensen (2002, May). NOTE: Thermal Emission Spectrometer Observations of Martian Planet-Encircling Dust Storm 2001A. *Icarus* 157, 259–263.
- Stark, G., K. Yoshino, P. L. Smith, and K. Ito (2007, January). Photoabsorption cross section measurements of CO₂ between 106.1 and 118.7 nm at 295 and 195 K. *J. Quant. Spec. Radiat. Transf.* 103, 67–73.
- Stephenson, J. D., L. J. Hallis, K. Nagashima, and S. J. Freeland (2013). Boron Enrichment in Martian Clay. *PLoS ONE* 8(6), 6–9.
- Tian, F., J. F. Kasting, and S. C. Solomon (2009, January). Thermal escape of carbon from the early Martian atmosphere. *Geophys. Res. Lett.* 36, L02205.
- Toon, O. B., C. P. McKay, T. P. Ackerman, and K. Santhanam (1989, November). Rapid calculation of radiative heating rates and photodissociation rates in inhomogeneous multiple scattering atmospheres. *J. Geophys. Res.* 94, 16287–16301.
- Victor, G. A. and A. Dalgarno (1969, March). Dipole Properties of Molecular Hydrogen. *J. Chem. Phys.* 50, 2535–2539.
- Vincendon, M., C. Pilorget, B. Gondet, S. Murchie, and J.-P. Bibring (2011, November). New near-IR observations of mesospheric CO₂ and H₂O clouds on Mars. *Journal of Geophysical Research (Planets)* 116, E00J02.
- Voet, D., W. B. Gratzer, R. a. Cox, and P. Doty (1963, June). Absorption spectra of nucleotides, polynucleotides, and nucleic acids in the far ultraviolet. *Biopolymers* 1(3), 193–208.
- Wagner, W. and A. Pruß (2002, June). The IAPWS Formulation 1995 for the Thermodynamic Properties of Ordinary Water Substance for General and Scientific Use. *Journal of Physical and Chemical Reference Data* 31, 387–535.
- Wagner, W., A. Saul, and A. Pruss (1994, May). International Equations for the Pressure Along the Melting and Along the Sublimation Curve of Ordinary Water Substance. *Journal of Physical and Chemical Reference Data* 23, 515–527.
- Warren, S. G. and R. E. Brandt (2008, July). Optical constants of ice from the ultraviolet to the microwave: A revised compilation. *Journal of Geophysical Research (Atmospheres)* 113, D14220.

- Wolff, M. J., M. D. Smith, R. T. Clancy, R. Arvidson, M. Kahre, F. Seelos, S. Murchie, and H. Savijärvi (2009, June). Wavelength dependence of dust aerosol single scattering albedo as observed by the Compact Reconnaissance Imaging Spectrometer. *Journal of Geophysical Research (Planets)* *114*, E00D04.
- Wordsworth, R., F. Forget, E. Millour, J. Head, J.-B. Madeleine, and B. Charnay (2013). Global modelling of the early martian climate under a denser CO₂ atmosphere: Water cycle and ice evolution. *Icarus* *222*(1), 1–19.
- Wordsworth, R., F. Forget, E. Millour, J. W. Head, J.-B. Madeleine, and B. Charnay (2013, January). Global modelling of the early martian climate under a denser CO₂ atmosphere: Water cycle and ice evolution. *Icarus* *222*, 1–19.
- Wordsworth, R., Y. Kalugina, S. Lokshtanov, A. Vigasin, B. Ehlmann, J. Head, C. Sanders, and H. Wang (2017, January). Transient reducing greenhouse warming on early Mars. *Geophys. Res. Lett.* *44*, 665–671.
- Wordsworth, R. D. (2016, June). The Climate of Early Mars. *Annual Review of Earth and Planetary Sciences* *44*, 381–408.
- Wordsworth, R. D., L. Kerber, R. T. Pierrehumbert, F. Forget, and J. W. Head (2015). Comparison of ”warm and wet” and ”cold and icy” scenarios for early Mars in a 3-D climate model. *Journal of Geophysical Research E: Planets* *120*(6), 1201–1219.
- Yoshino, K., J. R. Esmond, Y. Sun, W. H. Parkinson, K. Ito, and T. Matsui (1996, January). Absorption cross section measurements of carbon dioxide in the wavelength region 118.7-175.5 nm and the temperature dependence. *J. Quant. Spec. Radiat. Transf.* *55*, 53–60.
- Zurek, R. W. (1978, August). Solar heating of the Martian dusty atmosphere. *Icarus* *35*, 196–208.

A. Supplementary Figures

This appendix presents sample atmospheric profiles calculated using the methods in Section 3.2, to illustrate the application of these methods. Figure 23 shows the T/P profiles associated with a sample atmosphere with varying $(p\text{CO}_2, T_0)$, where $p\text{CO}_2$ is the surface partial pressure of CO_2 . Figure 24 shows the pressure, temperature, and H_2O molar concentration altitude provides associated with an atmosphere with $T_0 = 250$ K and varying $p\text{CO}_2$.

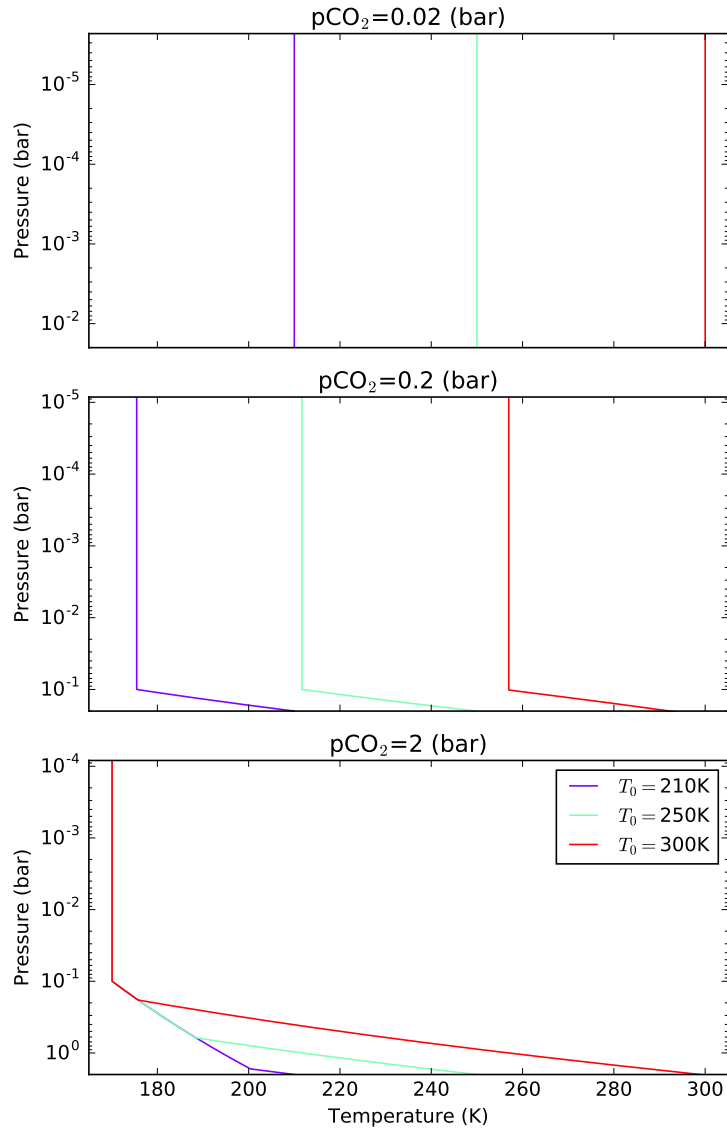


Fig. 23.— Sample T/P profiles for CO_2 -dominated CO_2 - H_2O atmospheres using the methodology in Section 3.2 for $T_0 = 210, 250, 300\text{K}$ and $p\text{CO}_2 = 0.02, 0.2, 2$ bar. The pressure is the total atmospheric pressure (CO_2 and H_2O).

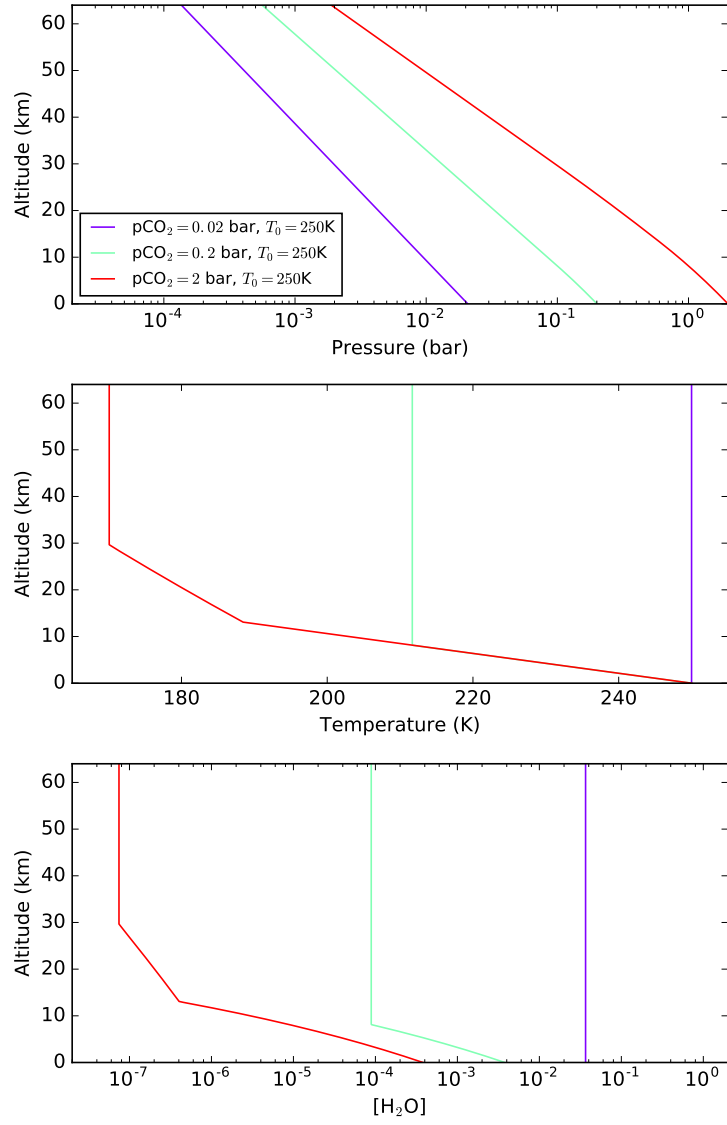


Fig. 24.— Temperature, pressure, and molar concentration of H_2O for atmospheres with $pCO_2 = 0.02, 0.2, 2$ bar and $T_0 = 250K$.